

THESIS ON CHEMISTRY AND CHEMICAL ENGINEERING G25

**Methodology and Equipment for  
Optical Studies of Fast Crystallizing Polymers**

TRIIN MÄRTSON

**TUT**  
**PRESS**

TALLINN UNIVERSITY OF TECHNOLOGY  
Faculty of Chemical and Materials Technology  
Department of Polymeric Materials

The dissertation was accepted for the defence of the degree of Doctor of Philosophy in Engineering on the 29<sup>th</sup> of January, 2010.

**Supervisor:**

Ph. D. Andres Krumme, Department of Polymeric Materials, Tallinn University of Technology

**Co-supervisor:**

Prof. Anti Viikna, Department of Polymeric Materials, Tallinn University of Technology

**Opponents:**

Prof. Jaan Roots, Department of Chemistry, University of Oslo, Norway

Ph. D. Arvo Mere, Institute of Physics, Tallinn University of Technology

**Defence of the thesis:** 1<sup>st</sup> March 2010 at 14:00, TUT main building VI-229

Declaration

Hereby I declare that this doctoral thesis, my original investigation and achievement, submitted for the Degree of Doctor of Philosophy at Tallinn University of Technology, has not been submitted for any academic degree.

/signature/

Copyright: Triin Märtson, 2010

ISSN 1406-4774

ISBN 978-9985-59-970-9

KEEMIA JA KEEMIASTEHNIKA G25

# **Metoodika ja seade kiirelt kristalluvate polümeeride optilisteks uuringuteks**

TRIIN MÄRTSON

## CONTENTS

INTRODUCTION.....	6
LIST OF ORIGINAL PAPERS .....	8
ABBREVIATIONS.....	9
1. LITERATURE SURVEY .....	11
1.1. Polymer crystallization.....	11
1.1.1. Crystal morphology and crystallinity .....	11
1.1.2. Crystallization process and its kinetics.....	12
1.1.3. Crystallization rate vs temperature (various polymers).....	14
1.2. Cooling rate at processing.....	16
1.3. Commercial hot stages .....	16
1.4. Unique solutions of rapid cooling .....	17
1.4.1. Gas-heated and -cooled hot-stage.....	17
1.4.2. Thin slice technique .....	18
1.4.3. Oven heating - spray cooling.....	18
1.4.4. Thin film sensors.....	18
1.5 Theoretical considerations.....	19
1.6. Deposition of thin films.....	19
2. EXPERIMENTAL .....	21
2.1. CNC and HS PLM measurements (gas-heated/cooled hot-stage)(II).....	21
2.2. <i>Inter experimentarum</i> – new conception (I).....	22
2.3. New generation of hot-stage – metal (gold) film heater/sensor (I).....	23
2.4. Improved design – metal oxide film heater, liquid flow cooling (III).....	24
2.5. Thermodynamic model of glass substrate .....	29
3.RESULTS AND DISCUSSION .....	32
3.1. Applicability of diverse methods – CNC vs HS PLM (II).....	32
3.2. Gas cooling.....	34
3.3 Transparent heater – gold and other metals <i>versus</i> ITO .....	36
3.4. Thermal tests on ITO-coated glasses.....	36
3.5. Results of modelling the substrate glass.....	37
3.6. Parameters of the controller .....	39
3.7. Output signal, temperature calibration .....	39
3.8. Experimental time constants vs theoretical .....	41
4. CONCLUSIONS.....	45
REFERENCES.....	46
KOKKUVÕTE.....	49
ABSTRACT .....	51

## INTRODUCTION

Polymer products are formed through solidification, which (in case of semicrystalline polymers) is to a large extent about crystallization. The metastable morphology arising at the low temperatures applied during industrial processing largely determines the product's mechanical and other application-related properties, e.g. endurance. It is, thus, of practical importance, in view of working out modified materials with new qualities, to simulate and systematically study the crystallization process at low temperature (high supercooling). Thermoplastic materials of different chemical structure (distribution of charges), geometry of chain etc. exhibit great differences in their inherent crystallization rates. The most widely used plastic material polyethylene with its simple and flexible chain is among the fastest crystallizing ones, together with polytetrafluoroethylene, polyamides, polylactic acid etc. Although it often serves as a model material for understanding the behaviour of polymeric materials as such, the high inherent crystallization rate sets limitations (or higher methodological requirements) to its studies at lower temperature, where the rate increases considerably.

As crystallization is very sensitive to temperature, it is important to have a measure enabling fast and precisely controlled changes of temperature – a hot-stage (or a „heating and freezing stage“). There are several hot-stage models commercially available, with a maximum cooling and heating rate of 100-150 K/min. Nevertheless, such a cooling rate would not suffice for crystallization studies of polymers with a fast crystallization rate under higher supercooling, instead some better solution is needed. Depending on the particular material and the process, the cooling rates to be applied are considerably (tens or even hundreds of times) higher. In the literature some interesting examples of unique devices are reported, but each of them has certain limitations (e.g. no actual temperature control – cooling only, or cooling agents that disturb simultaneous microscopic observations).

Hence the objective of this study to work out a novel design of a device and a methodology for routine measurements of very fast temperature-dependent processes, crystallization beforehand, ensuring fast and precise controlled change of the temperature of a polymer sample and enabling one to follow its morphological changes by optical methods, i.e. implying transparency. The aim is, thus, to broaden the applicability conditions of optical measurements closer to the realistic ones.

Looking into the constructional features of the available hot-stages – the working part mostly being a massive metal plate with the heating and cooling element and the temperature sensor at a distance from the sample – and, to the end of doing away with the functional limitations (thermal lag) coming thereof, the attempts were aimed at:

- 1) reducing the *addendum* mass (2-3 orders of magnitude) and dimensions
- 2) maximizing thermal contact (direct heating and temperature measurement)

3) increasing the cooling efficiency (10 times) and stability by picking out suitable materials and dimensions of the elements (holder, heater, temperature sensor, cooler), having also in mind the need for direct microscopy observations, assemble the whole system and test it for the performance of changing temperature, tests including heat resistance, cooling rate, temperature sensitivity, speed tests of the control unit and the whole system.

The results of the work have been published in an Estonian patent and two articles listed below.

Hereby I would like to render my thanks to kind persons who had a discernible positive influence on the success of my study – to supervisor Andres Krumme for inspiration and continuous support and his contribution in programming, to Ando Ots for his support and advice and contribution in electronics, to Ants Lõhmus for advice and assistance in a wide range of engineering matters, to Arne Kasikov and Tiit Varema for performing coatings, to Martin Timusk for calibrations, to Valter Kiisk for advice in thermodynamics, to Veljo Sinivee and Lembit Kurik for advice in electronics and physics. The Estonian Science Foundation is acknowledged for support under grant No. 6533, as well as Graduate School of Tartu University and Tallinn University of Technology “Functional Materials and Technologies”.

## LIST OF ORIGINAL PAPERS

This dissertation is based on the following publications (reprints appended), referred to by their Roman numerals in the text:

- I A. Krumme, M. Timusk, T. Märtson, R. Lõhmus, A. Lõhmus. Method and device for ultra fast temperature switch for microscopic objects. EE 05250 B1
- II T. Märtson, A. Krumme, V. Gavrilkina, A. Viikna. The effect of modality on linear low-density polyethylene crystallization behaviour at high and very high supercoolings. *Proceedings of the Estonian Academy of Sciences*, 2009, **58**, 1, 53-57
- III T. Märtson, A. Ots, A. Krumme, A. Lõhmus. Development of a faster hot-stage for microscopy studies of polymer crystallization. *Polym. Testing*, 2010, **29**, 1, 127-131

### **The author's contribution to the appended publications:**

- I The author participated in working out the principles and composing the text.
- II The author performed the crystallization measurements, partly together with V. Gavrilkina, did the calculations, drew the graphs, interpreted the results and wrote the paper.
- III The author participated in designing the body, designed the heaters, performed the tests and calculations, interpreted the results and wrote the article, integrating the contribution from A. Ots.

## ABBREVIATIONS

### Latin symbols

<i>Au</i>	gold
<i>E<sub>d</sub></i>	activation energy of diffusive transport
<i>G</i>	growth rate; free energy
<i>H</i>	enthalpy
<i>K</i>	crystallization rate constant
<i>L</i>	lamella thickness
<i>M</i>	mass
<i>N</i>	nucleation density
<i>Ti</i>	titanium
<i>T</i>	temperature
<i>T<sub>g</sub></i>	glass transition temperature
<i>T<sub>m</sub></i>	melting temperature
<i>T<sub>m</sub><sup>0</sup></i>	equilibrium melting temperature
<i>T<sub>∞</sub></i>	temperature at which all segmental mobility is frozen in
<i>V</i>	voltage; volume
<i>X</i>	degree of crystallinity
<i>c</i>	heat capacity
<i>h</i>	heat of fusion
<i>k</i>	Boltzmann constant
<i>n</i>	Avrami index
<i>q</i>	cooling rate
<i>t</i>	time
<i>v</i>	crystallization rate

### Subscripts

$\infty$	end
<i>cntr</i>	control
<i>crit</i>	critical
<i>cryst</i>	crystal
<i>e</i>	basal surface; etalon
<i>f</i>	fusion
<i>g</i>	glass transition
<i>h</i>	heating
<i>m</i>	melting
<i>max</i>	maximum
<i>min</i>	minimum
$\check{s}$	reference resistor

## Greek letters

$\Delta$	difference
$\beta$	pseudolinear temperature scan rate
$\alpha$	temperature coefficient of resistivity
$\kappa$	heat conductivity; temperature constant of crystal growth rate
$\rho$	density
$\sigma$	surface free energy,
$\tau$	time constant of cooling

## Acronyms

AFM	atomic force microscopy
CNC	chip nanocalorimetry
DSC	differential scanning calorimetry
DAQ	data acquisition and control board
HDPE	high density polyethylene
HMM	high molar mass
HS	hot stage
LDPE	low density polyethylene
LLDPE	linear low density polyethylene
LMM	low molar mass
LPE	linear polyethylene
MM	molar mass
MMD	molar mass distribution
PA	polyamide
PC	personal computer
PE	polyethylene
PET	polyethylene terephthalate
PID	proportional-integral-differential
PLA	polylactic acid
PLM	polarized light microscopy
PP	polypropylene
iPS	isotactic polystyrene
SCB	short chain branching
SCBD	short chain branching distribution
TEM	transition electron microscopy

## 1. LITERATURE SURVEY

### 1.1. Polymer crystallization

#### 1.1.1. Crystal morphology and crystallinity

Solid morphology is the main factor influencing the properties of a semicrystalline polymer. The morphology depends on the molecular structure – chemical structure, linearity (only the shortest branches can be normally included in crystals), flexibility, regularity [1], altogether influencing the crystallization capability and behaviour, on one hand, and conditions of crystallization on the other. Different polymers have different packing of chains – polyethylene, polyamides, polyester etc. have extended zig-zag (planar) chains, isotactic polypropylene, isotactic polystyrene etc. with large side groups have a helical packing [2]. Flexible chains can form random coils or fold into lamellar plates [3] or align into microthreads, rigid chains will form rodlets. Under very high pressures flexible chains may also form rodlets.

Various superstructures are formed of *lamellae*, depending on the molar mass and crystallization conditions. Typically a single dominant *lamella* (under quiescent conditions) grows radially, regularly splays in the direction of the fastest growth due to screw dislocations. The explanation to this is the short-range repulsion of partly crystallized molecules, i.e. dynamic *cilia*. A young superstructure is sheaf-like, becoming spherical in the end – a spherulite. At higher temperatures, when branching frequency is low, axialites precede spherulites [4]. Axialites may be observed in place of spherulites, where the volume available for growth is limited due to high nucleation density [5]. Microthreads (under shear) develop into a row-nucleated lamellar structure with a fibrillar core (extended chains to the direction of strain) and perpendicular lamellar periphery (*shish-kebab*). Very dilute solutions yield plate-like lamellar single crystals or hollow pyramids. At lower crystallization temperatures the *lamellae* also turn out curved or S-shaped [6,7]. Very high molar mass polyethylene crystallizes in irregular spherulites or only random *lamellae* [8]. Size of the superstructures is also MM dependent in the spherulite forming MM range [9].

Polymers capable of crystallization are called semicrystalline because there is always a certain portion of material that is left out of the *lamellae* – branches, loops, entanglements, tie molecules (i.e. chains extending from one *lamella* to another). Three different structural regions are distinguished between in a semicrystalline polymer – aside from the crystallite and the amorphous interlamellar region there is the interfacial region comprising chain folds [10].

Crystalline polymers have a broad melting and crystallization range consisting of a series of melting points that correspond to the melting of *lamellae* of various

thickness. Thicker *lamellae* have higher melting points due to thermodynamic reasons. The dispersion of *lamella* thickness is a consequence of entanglements and chain branches that divide chain backbones into a series of discrete crystallizable sequences with a distribution of lengths. Low MM LPE crystallized in isothermal conditions has the narrowest melting range [11].

*Lamella* thickness  $L$  and melting temperature  $T_m$  are bound by Thomson – Gibbs equation [12,13]  $T_m = T_m^0 \left(1 - \frac{2\sigma_e}{\Delta H_f L}\right)$ , where  $T_m^0$  is the equilibrium melting temperature,  $\Delta H_f$  the fusion enthalpy of the crystalline phase and  $\sigma_e$  the surface free energy of the basal surface of the crystalline *lamella*. Branching tends to reduce *lamella* thickness, as branches are excluded from the *lamella* [14,15]. The melting temperature increases with MM especially in the lower MM range (MM < 10 kg/mol) [16,17,18].

The ratio of crystallized matter is the degree of crystallinity  $X$ . Other parameters characterizing crystallization are nucleation density  $N$  (number of nuclei or crystalline entities per volume unit) and spherulite radius  $r$ .

### 1.1.2. Crystallization process and its kinetics

Crystallization involves diffusion of the crystallizable units to the crystal front and nucleation [3]. (Growth of crystal also proceeds by the nucleation mechanism [2].) Short-range diffusion is faster at higher temperatures. All diffusive motions are „frozen in“ at temperatures below the glass transition temperature. When the diffusing molecule reaches the crystal boundary, it has to form a stable *nucleus*. Stability conditions are described by nucleation theory. Below the equilibrium melting temperature  $T_m^0$  the surface energies  $\sigma_i$  (different for every surface  $i$ ) make up for the crystallization free energy (related to the volume of the crystal)  $\Delta g V_{cryst}$ . Hence the tendency for crystallites to be spherical, in this case the increase in free energy is  $\Delta G = \Delta g \frac{4\pi r^3}{3} + 4\pi r^2 \sigma$ , where  $r$  is the radius of the crystallite. The radius of the critical nucleus  $r^*$  can be found if the derivative of the free energy with respect to radius is set to zero:  $4\pi r^{*2} \Delta g = -8\pi r^* \sigma$  and  $r^* = -2\sigma/\Delta g$ . It depends on temperature, so far as  $\Delta g$  is proportional to supercooling  $\Delta T = (T_m^0 - T)$ . Provided the heat of fusion  $\Delta h^0$  is temperature-independent,  $r^* = -2\sigma T_m^0 / \Delta h^0 \Delta T$ . The heat of fusion is negative and the critical nucleus has to be the larger, the closer to the equilibrium melting point. The free energy barrier of nucleation can be expressed in a concise form  $\Delta G^* = 16\pi\sigma^3 (T_m^0)^2 / 3(\Delta h^0)^2 \Delta T^2$ . Thus, nucleation is favoured at lower temperatures due to the smaller critical nucleus size and lower free energy barrier.

Primary (homogeneous) nucleation is the spontaneous formation of a *nucleus* in the absence of a second phase, due to fluctuation of density and order only, secondary *nucleus* is formed on an existing surface (interphase of the growing phase) and tertiary between two existing surfaces (lesser dimensionality). The free energy

barrier is highest for primary nucleation and, thus, homogeneous nucleation occurs very seldom (it takes 50-100 K of supercooling to make it happen). In all practical cases crystallization starts from the formation of a secondary nucleus on some impurity, nucleating additive or residue of incomplete melting (of the higher MM component) [6], followed by a series of tertiary nucleation acts.

Crystallization can be divided into two separate *phenomena* (again primary and secondary) – during primary crystallization the complete volume of the melt is converted into a solid but crystallinity continues to increase during secondary crystallization on account of thickening of *lamellae*, reorganization of the crystal lattice, crystallization of the matter that has grown in but remained amorphous. Secondary crystallization is slower, so after primary crystallization is finished, the crystal growth rate decreases. Still, secondary crystallization starts before primary is completed. Around 40 % of crystallinity is formed during the secondary process [19] and the influence of secondary crystallization increases with higher MM [20].

When considering the rate of crystallization, not only the nucleation free energy barrier, but the number of available *nuclei* and the rate of diffusive transport has to be taken into account – close to the melting point the nucleation energy barrier is very high, close to the glass transition point, diffusion is very slow, so at these points the rate is zero. Between  $T_g$  and  $T_m$ , growth rate (and resulting properties) are temperature-dependent. The growth rate is theoretically expressed [21] by  $v = v_0 \exp(-E_d/R(T-T_\infty)) \exp(\Delta G/kT)$ . As experimental data [22] show that the activation energy of diffusive transport  $E_d$  increases monotonically with  $T_g$  and the free energy of a *nucleus* is also empirically related to the characteristic transition temperatures, it can be expressed in more empirical terms  $v = v_0 \exp(-E_d/R(T-T_\infty)) \exp(-K_g/T(T_m-T))$ , where  $R$  is the gas constant,  $K_g$  is the kinetic constant for secondary nucleation,  $T_\infty$  is the temperature at which all segmental mobility is frozen in (approximately  $T_g - 50$  K for most thermoplastics [23]). The constant  $v_0$  is independent of temperature, still it has proved to depend on MM [24], furthermore, [3] it depends on segmental flexibility and regularity, e.g. iPS is very rigid and crystallizes slowly.

The rate generally decreases with the increase of average MM [6,25-30], but the dependency is not single-valued and it depends on other conditions [28,20]. This is explained by different mechanisms that control the crystallization rate – in the lower MM range crystallization is mostly controlled by the rate of secondary nucleation (the rate at which a new chain deposits to the crystallizing surface) [40,28], with higher MM the effect of chain mobility (melt viscosity) and topological impurities dominates (diffusion of longer chains to the crystallization front is slower and hindered by entanglements, loops, knots etc present in the melt and are rejected from the crystalline phase [6,25,26]. Thus, the nucleation-controlled rate and the diffusion-controlled rate may have different MM dependences.

A convenient equation to describe *inter alia* time evolution of overall crystallinity is that of Avrami  $1-X=\exp(-Kt^n)$ , where  $K$  is the rate constant at a particular temperature and  $n$  is the Avrami *index* indicative of the dimensionality of the growth and nucleation mechanism, e.g.  $n$  is 1 for athermal nucleation (all *nuclei* are initiated at once) and linear growth, 2 for circular and 3 for spherical growth, thermal nucleation adds 1 to  $n$ , diffusion control reduces it to half the value. In reality the mechanism is mixed and values of  $n$  are not integer. The equation can be simplified for early stages of crystallization with no impingement:  $X=Kt^n$  (Göler equation). To take into account the fact that crystallinity in polymers can never be 100%, the initial expression is to be modified:  $1-X/X_\infty=\exp(-Kt^n)$ , where  $X_\infty$  is the final value of crystallinity. Experimental growth plot is sigmoid-shaped (e.g. Figure 3.4), if these data are expressed in a double logarithmic plot ( $\ln[-\ln(1-X/X_\infty)]$  versus  $\ln t$ ), the intercept of the initial straight part reveals the rate constant  $K$  at that particular temperature and the slope – the Avrami index. Another widespread and comprehensible expression of crystallization rate, both in calorimetry and microscopy, is the reciprocal of time to the moment when the growth is most intensive (e.g. exotherm peak in DSC or maximum of differential curves in polarized light microscopy), which has a temperature dependence close to linear.

### 1.1.3. Crystallization rate vs temperature (various polymers)

In order for isothermal crystallization measurements to be correct, the temperature of measurement has to be reached and stabilized before the bulk (99 %) of crystallization has not taken place yet. As explained in 1.1.2., the linear growth rate of crystals from the melt has a bell-like temperature dependence between  $T_g$  and  $T_m$  [32].

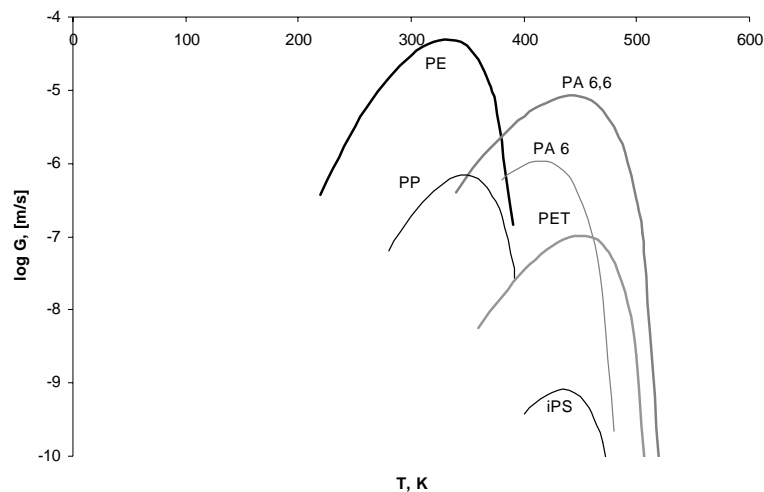


**Figure 1.1.** Temperature dependence of linear growth rate  $G$  of spherulites of various polymers (calculated)

Van Krevelen [2] has developed a very practical expression of crystal growth rate exclusively based on characteristic transition temperatures:

$$\log G(T) = \log G_0 - 2.3 \frac{\frac{T_m}{T}}{1 - \frac{T_g}{T_m}} - \frac{115 \left( \frac{T_m}{T} \right)^2}{T_m \frac{T_m}{T} - 1} \quad (1.1)$$

where  $G_0$  is a constant of an approximate value 750 m/s. Dependences for a set of thermoplastics are presented in Figure 1.1. It has also been shown [23] that all crystalline thermoplastics have the dependence congruent, coinciding in axes  $\log G/G_{\max}$  vs  $(T-T_g+50)/(T_{\max}-T_g+50)$  (Figure 1.2), where  $T_{\max}$  is the temperature at which the linear growth rate is at its maximum  $G_{\max}$ .  $T_g-50$ , also designated as  $T_\infty$ , denotes the temperature where all segmental mobility is frozen in.

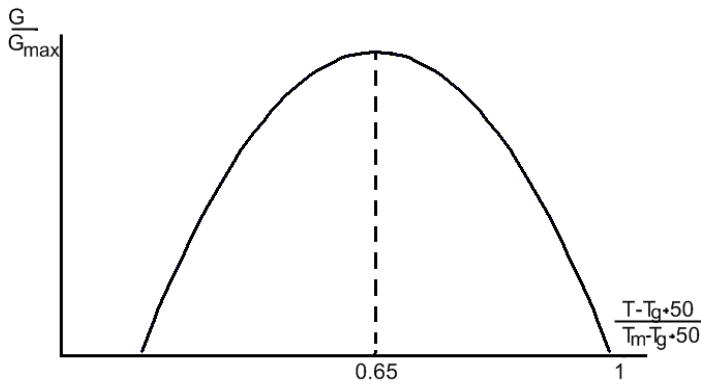


**Figure 1.2.** Dimensionless master curve of growth rate for all thermoplastics (schematic)

To estimate the critical cooling rate necessary for reaching the measurement temperature ahead of 99 % of the crystallization process, Eder [33] has theoretically derived the following expression:

$$q_{crit} = 13.24 \frac{G_{\max} \sqrt[3]{N_{\max}}}{\kappa}, \quad (1.2)$$

where  $N_{\max}$  is the maximum nucleation density (characteristic of a material, e.g.  $10^{17} \text{ m}^{-3}$  for polyethylene,  $10^{15} \text{ m}^{-3}$  for many other thermoplastics) and  $\kappa$  the temperature constant of crystal growth rate (varying from  $0.01 \text{ K}^{-1}$  to  $0.1 \text{ K}^{-1}$  depending on the material). Inserting these values and the value of  $G_{\max}$  calculated from (1.1) into (1.2) one can find out how fast the sample has to be cooled to be able to perform the crystallization analysis at a desired supercooling.

## 1.2. Cooling rate at processing

During industrial processing (solidification of melt into products) polymer materials are subjected to fast cooling, depending on the particular process [34], examples of applied cooling rates are in Table 1. It is not only due to economic (time saving) reasons – plastic materials are known to be brittle, when spherulites are large. To get many small spherulites and as much as possible tie molecules or other in-frozen amorphous matter, it is advantageous in general to cool fast [3].

Table 1. Cooling rates in industrial polymer processing

Process	cooling rate, K/min
Rotation moulding	70
Extrusion	125
Injection moulding (core)	250
Injection moulding (skin), film blowing, fibre spinning	400 and higher

In order to simulate and systematically study these processes one needs equipment (hot-stage) for controlled heating and cooling at the given rate or, for isothermal analysis (which gives more comprehensible information), even at a faster rate.

## 1.3. Commercial hot stages

Several kinds of hot-stages are commercially available, Linkam THMS600 [35] is one of the most efficient heating and freezing stages for microscopy. Samples together with a thin (0.17 mm) glass cover slip are heated on a silver heating element, temperature is measured by a platinum resistor sensor. The resistor being more accurate and the signal more stable than that of a thermocouple, it still forcibly measures the temperature of the sample through the heater and the glass. Besides, neither heating nor temperature measurement can be directly beneath the sample, because there has to be a hole for the light beam. So the heat from the heater to the sample and back to the temperature sensor is transferred either through glass lengthwise or through air and glass crosswise, causing a considerable thermal lag – maximum heating and cooling rate is 150 K/min. Mettler Toledo FP82HT/84HT hot-stage [36] yields a heating and cooling rate 20 K/min as a maximum. Comparing these data with Table 1, one can see that these devices can be applicable for crystallization analysis imitating extrusion or at best rotation moulding, but not for injection moulding or film blowing.

In calorimetry the most efficient commercial models (e.g. Perkin Elmer Hyper DSC [37], yet not applicable for optical analysis) develop a linear scanning rate up to 500 K/min .

## 1.4. Unique solutions of rapid cooling

### 1.4.1. Gas-heated and -cooled hot-stage

To overcome the disadvantages related to solid heat exchangers of commercial hot stages, a couple of gas-heated and -cooled unique devices are described. The unique fixture in [36] (Figure 1.3) holds the 2  $\mu\text{m}$  sample between glass slips of 0.14 mm and the sample temperature is changed by means of nitrogen gas flow from below. The gas is heated electrically and the heating voltage controlled by a virtual instrument using PID algorithm. Miniature (10  $\mu\text{m}$  wire) E type (Chromel vs Constantan) thermocouples are on either side of the glass-sample-glass package, symmetrically to the sample, and their average is the sample temperature.

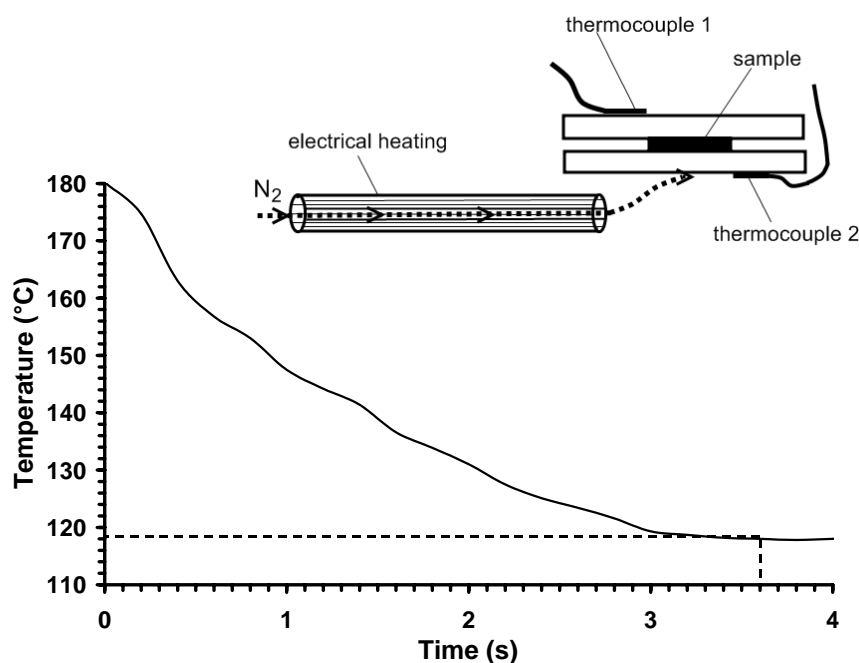


**Figure 1.3.** Principle of heating and cooling (top right) and an example of cooling curve of the gas-heated and -cooled hot-stage

It is considerably faster than the commercial stages – 17 K/s or 1000 K/min. But limitations like heating through glass, critical thermal contact with the upper thermocouple (the lower is in the gas ambient anyway), would not allow studies at larger supercooling. The PID algorithm avoids undershoot, but it slows down the cooling when the set-point approaches. The lowest isothermal analysis temperature the device reached before discernible crystallization of LMM PE started, was 109°C. When the set-point was 108°C, crystallization of the sample started already during the cooling phase. This allows approximately 12 K lower isothermal analysis temperature for PE than Mettler Toledo FP82 hot-stage (maximum controlled cooling rate 0.33 K/s).

In [38] the 150  $\mu\text{m}$  thick polymer sample, with a small thermocouple inside, between two glasses, is heated and cooled by flowing gas from both sides, the reported cooling rate 2500 K/min allows polypropylene analysis down around 90°C.

#### **1.4.2. Thin slice technique**

In [39] a device is described consisting of a massive heated cell with the sample sandwiched between two thin glasses at a distance from the heaters. The cell is flushed with a fluid at the crystallization temperature for a certain crystallization time and then flushed with ice water to stop crystallization. The crystals are observed *post factum*. This device is applicable with materials of a crystal growth rate not exceeding 10  $\mu\text{m/s}$  and the growth cannot be observed in real time.

#### **1.4.3. Oven heating - spray cooling**

In order to obtain real time experimental data of polymer crystallization at high cooling rates, an apparatus was worked out and tested in [40] – the sample was quickly shifted from the electric oven zone to the liquid (water) spraying zone, fast thermocouples were inserted in the 50-100  $\mu\text{m}$  thick sample itself, yielding a cooling rate of 35 K/s. The described temperature control mechanism is one-way (no heating is applicable after the shift), the sample is too thick to allow fast cooling inside, besides a sophisticated optical setup is required to eliminate the disturbing light scattering from the sprayed liquid. This apparatus could fit for crystallization analysis of polypropylene and other polymers with a medium crystallization rate.

#### **1.4.4. Thin film sensors**

A super fast hot stage (scan rate 100,000 K/s) is described in [41], based on a 30 micron  $\text{Si}_3\text{N}_4$  membrane with a deposited bifunctional 50 nm Pt film (no indication on the technology of Pt depositing process), dimensions 0.5 x 5 mm. Crystals are grown from a diluted xylene solution 125°C by self-seeding – first quenching on ice-water, then slowly heated to 99°C and left in oil bath of 70°C. The grown crystals in the solution are sprayed to the membrane sensor by an airbrush at slow velocity to allow the solvent to evaporate, thereafter calorimetric measurements are made and crystals observed in AFM and TEM. In this work cooling is not controlled – instead quenching is used, and optical methods are not applied during crystal growth.

In [42] the author warns for capacitive and inductive coupling between heating and temperature sensing components, even when they are electrically isolated, especially at short time intervals. In his set-up the same electrical component, a resistor, acts as a heater and temperature sensor, a super low temperature heat sink is used with a heat conductive layer of  $\text{N}_2$  or He gas between the resistor film and the heat sink.

For calorimetric studies of small samples [43-45], in order to increase time resolution and signal to noise ratio, the mass of the measuring system is reduced by using calorimetric chips capable of heating the sample and cooling it down to the surroundings temperature at a rate of  $10^6$  K/s. Some chip models are applicable for optical studies as well [44]. In chapters 2.1 and 3.1 of this thesis some examples are brought – sample handling with these fragile and expensive chips cannot be called a routine procedure, besides the calibration is very complicated, but the principles can be used in a more accessible way.

### **1.5 Theoretical considerations**

Proceeding from the comparison of devices and techniques reported in the literature the conception of a new design can be formed. Fast cooling is possible where thermal *inertia* is minimized on account of a drastic mass reduction. For more efficient heat transfer the sample-holder itself has to be the heater. Temperature measurement in very fast calorimetric systems is done either by microscopic thermopiles or by resistivity sensors. The resistor acting as a temperature sensor helps to reduce the time constant. In calorimetric systems the support, the heater and the cooler need not necessarily be transparent – e.g. a super low temperature heat sink is not. In optical applications transparency has to be paid extra attention. And even if a micron level membrane is more or less transparent, whatever its material, for a routine measurement procedure, somewhat more robust components are to be used with extra good transparency – conductive glass or glass with a conductive coating.

### **1.6. Deposition of thin films**

A technique for depositing thin films is physical sputtering – incident ions from a plasma, an accelerator or a radioactive material cause collision cascades in the target. When the cascade reaches the target surface and its energy exceeds the surface binding energy, an atom can be ejected. The average number of atoms ejected from the target per incident ion – the sputter yield, depends on the incident angle, the energy and mass of the ion, the mass of the target atoms and their surface binding energy, the orientation of the crystal axes is also relevant [46].

In thermal evaporation deposition the material is melted in a radiatively heated crucible or hung from an electric filament and evaporated from a hot source in a vacuum (to allow vapour particles to travel as directly as possible to the target object or substrate) and let condense there. The heating filament itself produces unwanted vapours that limit the quality of the vacuum. If a metal is deposited in the presence of oxygen, some oxide is formed on the substrate.

In electron beam evaporation the source is bombarded with an electron beam from a tungsten filament electrode. The source atoms form a gas which is condensed evenly on the substrate and chamber walls. The thickness of the film will vary due

to the geometry of the evaporation chamber. Electron-beam evaporation allows tight control of the evaporation rate.

Sputtering has better step coverage (no material in the shadows of the mask) and tends to deposit material more slowly than evaporation. Sputtering produces many high-speed atoms that bombard the substrate and may damage it. Evaporated atoms have a Maxwellian energy distribution, determined by the temperature of the source, which reduces the number of high-speed atoms, whereas electron beams tend to produce X-rays and stray electrons, which can also damage the substrate [47].

## 2. EXPERIMENTAL

### 2.1. CNC and HS PLM measurements (gas-heated/cooled hot-stage)(II)

A comparative crystallization study was made on a pair of LLDPE materials by means of two methods. For chip nanocalorimetry (first introduced by Schick *et al* [45]) XEN-39272 chip sensors by Xensor Integration were used – sensor dimensions 100x100  $\mu\text{m}$ , maximum nominal cooling rate  $10^5$  K/s and thermopile sensitivity 2 mV/K, which imply respectively small samples (2-5  $\mu\text{m}$  thickness). Polymer slices of 5  $\mu\text{m}$  were cut by ultramicrotome (Ultrotome 2128 by LKB), melted and pressed thinner between two microscopy cover slips and then cropped to 100x100  $\mu\text{m}$  by a surgical knife under microscope (the operator wore conductive clothing to prevent static repulsion and loss of the small polymer piece). After being lifted onto the sensor chip by means of bevelled thin Cu wires, the sample was manually subjected to a short heating pulse of 3 V to melt it and make it adhere evenly to the sensor surface. The sensor chip with the sample was placed into a unique temperature controlled furnace – a ceramic ring-shaped electrical heater in a relatively massive (90 g) brass body. Temperature of the furnace was measured by a resistance thermopile and controlled by means of an electronic temperature controller (TC200 Thorlabs) via a LabVIEW™ virtual instrument specially composed for this experiment. Prior to each series of measurements the furnace was flushed with nitrogen in order to avoid oxidation of the sample. At first a sharp heating pulse (2.3 V during 30 ms) was given to melt the sample, then the heating voltage of the calorimetric chip was switched off to make the sample cool down as fast as possible to the constant furnace temperature. Temperature signal from the sensor was recorded at 6000 points per second. Every measurement lasted for 1 second, stabilization of the furnace temperature on a new level took 1-5 minutes, depending on the temperature interval (2.5 through 10 K).

Although the microgram sample cools down in the 100 g furnace very fast, it still takes a finite time, so the starting moment of crystallization was counted not from the moment of turning-off of the heating voltage, but from the point where the steepest tangent to the cooling slope crosses the base line. Crystallization rate was estimated by the reciprocal of time to the local maximum of the temperature curve – the time moment when the exothermal effect of the crystallization process was the most intensive (Figure 2.1).

Hot-stage polarized light microscopy (HS PLM) measurements were done on the gas-heated/cooled unique hot stage [36] (described under 1.4.1) mounted on a light microscope Axioskop 2 by Zeiss. The sample was pre-melted at 180°C for 30 seconds in order to erase the thermal history and then cooled down to the chosen isothermal crystallization temperature by controlling the electrical heating of the nitrogen gas via PID. When the temperature reached the isothermal level, image grabbing was turned on, 150 images were taken at equal intervals (3 to 25 frames *per* second, depending on the time to saturation, which depends on the measurement temperature), the images being analyzed subsequently.

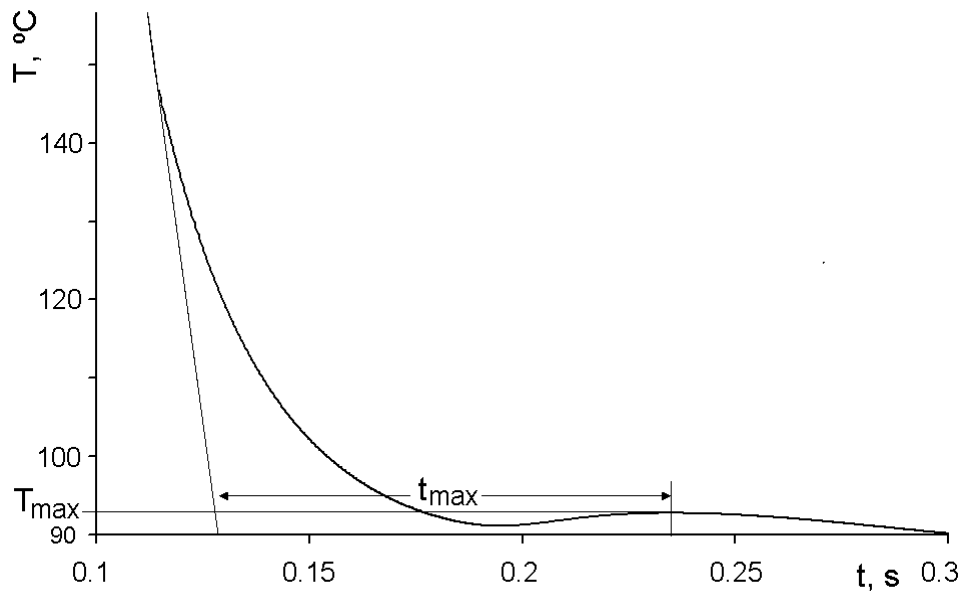


**Figure 2.1.** Temperature on the chip sensor – free cooling and crystallization exotherm. Graphical determining of the starting moment and rate of crystallization

## 2.2. *Inter experimentarum* – new conception (I)

Looking into the examples of available hot-stages, both commercial and unique ones, the mass of the *addendum* (support) and thus thermal *inertia* is definitely a hindrance to fast temperature movements of the sample, as well as insufficient thermal contact with the thermocouple or any other temperature sensor. If the thermocouple is embedded in the support, the temperature of the latter being considered to be the sample temperature is too far an approximation. To avoid these problems, it was decided that the support itself can be electrically heated (for optical applications it has to be transparent), that the mass of the heater has to be kept minimum and it has to be combined with immediate fluid cooling (to benefit from the effect of heat transfer *via* mass transfer). It is possible to heat and cool at the same time and to maintain the temperature of the sample constant at a required level by balancing the heating and cooling powers. Temperature can be changed by regulating only the heating voltage. Temperature control may be based on preliminary tests and calculations or on temperature feedback using PID algorithm (the latter may, though, somewhat prolong the time to the set-point). Temperature can be measured by using the temperature dependence of the electrical resistance of the same transparent heater – this eliminates problems with thermal lag and insufficient thermal contact.

### 2.3. New generation of hot-stage – metal (gold) film heater/sensor (I)

Based on the new conception, the first prototype (Figure 2.2) was designed, the centerpiece of which – a glass cover slip with a semitransparent vacuum-deposited gold strip and considerably thicker copper contact edges, serving as an electric heater and resistor sensor. The titanium body was meant to minimize thermal expansion (in order not to lose the focus of the short-focus-length objective). The gilded glass with the sample on top is inserted under copper sheet spring electrodes. For a stable contact, a drop of liquid In-Ga alloy or a soft whisk of In threads is inserted between the glass contact layer and the sheet springs.

Beneath the glass, supporting it from sagging when hot (thermal distortions caused focus problems initially), there is a circular cooler tube with 8 symmetrical vents directed towards the sample position, another cooler ring is fastened to the microscope objective. The coolers were devised to be used with some volatile liquid which, evaporating on the hot surface consumes energy, giving an extra cooling effect – that of phase transition. But as such volatile liquids tend to be highly flammable the cooler was never used in that way. Instead, nitrogen gas flow was used, cooled due to expansion while exiting the pressure bottle. The gas flow is kept constant and thus the whole periphery is kept cool during the measurement. The heat capacity of the sample and the heater was made as small as possible to be able to be easily cooled down by the gas flow as soon as the heating current drops.

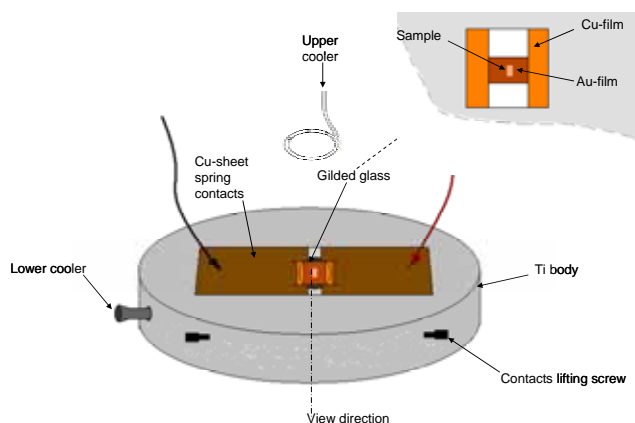


**Figure 2.2.** Hot-stage based on thin metal film heater/sensor

The gilded glass is used for one sample only. A batch of 25 glasses was deposited at a time and 2 or 3 of each batch were calibrated – temperature dependence of resistance was measured in a precision furnace. 3 batches of glass were used with initial resistivity varying between 7 and 35  $\Omega$ , rising for about 5  $\Omega$  from room temperature to 180  $^{\circ}\text{C}$ .

A 16 bit data acquisition and control board (DT9806 by Data Translation) operated by a LabVIEW™ virtual instrument was used for measuring and controlling temperature. In order to know the temperature one needs to know the resistivity of the gold film strip. For that, voltage on the gold film ( $V_1$ ) is measured and compared with the voltage on a precision reference resistor ( $V_2$ ). Voltage on the film resistor is  $R_{Au} = R_s V_1 / V_2$ , where  $R_s$  is the resistance of the precision reference resistor and  $T = T(R_{Au})$  according to the approximation formula of calibration.

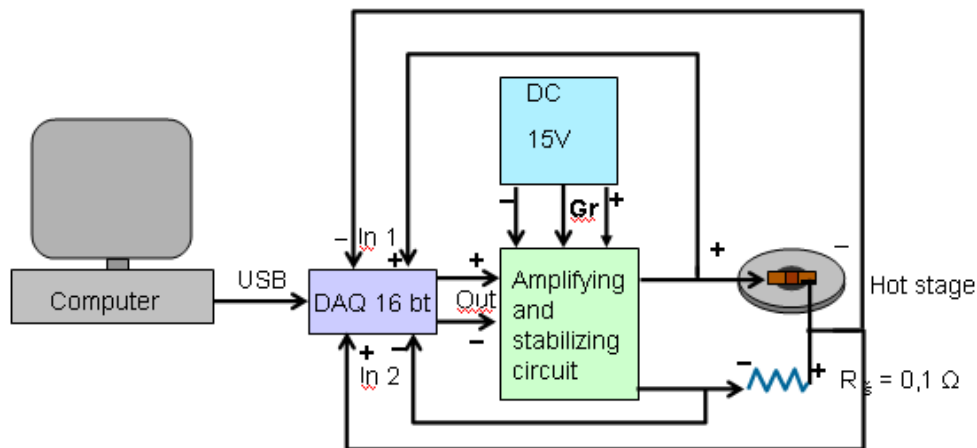


**Figure 2.3.** Block diagram of temperature measurement and control system for HS PLM

Isothermal measurements were made (although other temperature programs are feasible) – after deleting the thermal history at 160 - 180°C for 30 seconds, temperature was sharply lowered to the desired supercooling. The length of isothermal measurement periods varies (depending on when the radial growth curve turns towards saturation) from less than a second to ten minutes. Image analysis is also done by the LabVIEW™ virtual instrument. The crystallinity of the sample at any particular moment is assumed to be proportional to the intensity of light that passes through the crystallizing matter between two polarizers with their principal planes crossed, i.e. to the proportion of light pixels in the respective microscopy image (residual luminescence being subtracted). Crystallization rate is estimated by the reciprocal of time to the moment where crystal growth was the fastest (maximum of the differential curve).

#### **2.4. Improved design – metal oxide film heater, liquid flow cooling (III)**

Taking into account the disadvantages and inconveniences of the first prototype, beforehand the deficiencies of the thin gold layer and the inefficiency of gas cooling (as described in 3.3), the gold resistor was decided to be substituted with

some other metal or metal oxide and the new design was to be based on liquid flow cooling immediately under a thin coated glass heater (Figure 2.4 left).

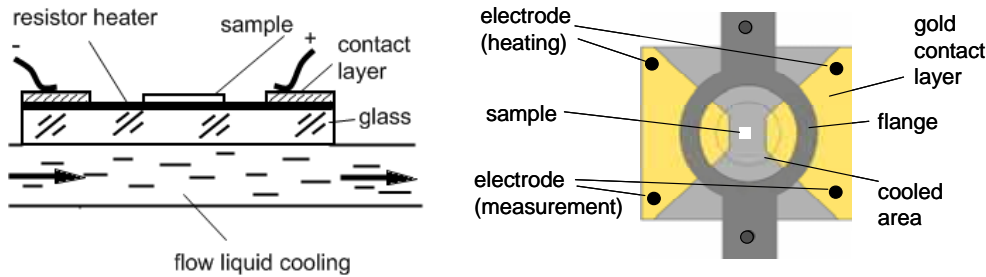


**Figure 2.4.** Transparent heater with liquid flow cooling, cross section (left), top view with gilded contact edges and flange (right)

Several heater materials and configurations were tested – fine spiral patterns photo-etched from a thicker vacuum-deposited copper layer, a continuous thin copper layer covered with  $\text{Al}_2\text{O}_3$ , an attempt was also made to deposit nickel. Indium titanium oxide (ITO) coated glass samples were tested for temperature dependence of resistance by means of the temperature measurement and control system described in 2.3 (Figure 2.3) and a K-type thermocouple at a rate of 1 min/5 K. Heating power was tested with 24 V and 30 V power supply units combined with room temperature cooling water circulated by MLW U2 thermostat. Thermal shock proof was done by manually changing the heating voltage at different rates and checking the temperature by a contact thermocouple.

Based on the results (in 3.4) of the above-mentioned tests and theoretical simulation of the glass substrate thickness (as described below, in 2.5 and results in 3.5), the transparent resistor heater/sensor (Figure 2.4. and 2 in Figure 2.5) was made of a 0.175 mm glass substrate with a ~100 nm ITO coating (nominal sheet resistance 20  $\Omega$ ) by Präzisions Glas & Optik GmbH, Germany. The ITO layer thickness (resistance) was chosen to yield a sufficient heating power  $P=V^2/R$  in combination with a maximum of 20 V heating voltage (considering that 10 V of the power supply is used by the controller itself), bearing also in mind the increased (liquid) cooling power to be balanced. The heated area between golden contact layers was made 3x3 mm.

The hot-stage design was improved (Figure 2.5) according to the above-mentioned considerations. There is a closed channel for the cooling liquid. Whilst the body of the previous model was so heavy as to stand firmly on the microscope stage without being fastened (nor moved), the new body was made exactly the length of a microscope slide glass and can be easily placed between the spring lugs of the fine positioning stage, facilitating precise movements of the sample. The heater is tightened against the body by a thermoresistant packing o-ring, flange and screws

(4, 5 and 6 in Figure 2.5), a thin mica ring isolator is between the flange and the ITO-layer.

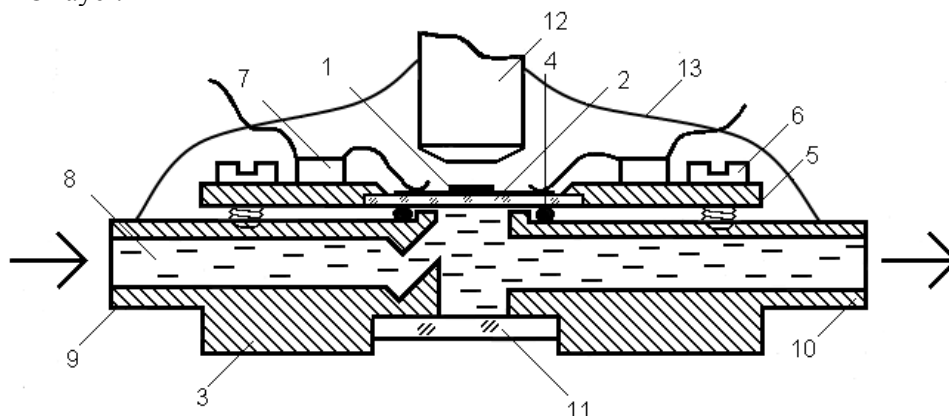


**Figure 2.5.** Improved design of hot-stage (schematic): 1) polymer sample, 2) transparent resistor heater/sensor, 3) body, 4) thermoresistant packing o-ring, 5) flange, 6) screws, 7) graphite electrodes, 8) cooling liquid (water or solution of ethylene glycole etc), 9) inlet nozzle, 10) outlet, 11) glass window, 12) objective, 13) rubber hood for inert gas

The cooling liquid (water solution of ethylene glycole or water) can be externally thermostated or circulated at room temperature 21°C (5 litres of circulating water proved not to warm discernibly within a couple of hours of measurements – the small quantity of heat is dissipated in the air). The flow of the liquid is directed against the substrate glass at ~45° angle to ensure the best cooling efficiency. For polymer samples with no antioxidant additives or for cooling liquid temperature lower than 10°C, a rubber hood can be used, tight round the objective, to be flushed with dry nitrogen gas, to avoid oxidation of the polymer sample or condensation of moisture.

The liquid is kept flowing at a constant rate throughout the experiment and, for temperature control, only the heating voltage is changed. The heating voltage is controlled by an analogue output of a PC-connected data acquisition board DT 9086 by Data Translation™ and a virtual instrument in LabVIEW™ (Figure 2.6).

As it is even more important than the cooling rate, to be able to detect the actual temperature of the sample and thus control the cooling, and, as the temperature dependence of resistance of ITO is weaker than with metals and the signal needs to be amplified out of possible noises, a special multifunctional temperature measuring and control unit (Figure 2.7) was designed (III).

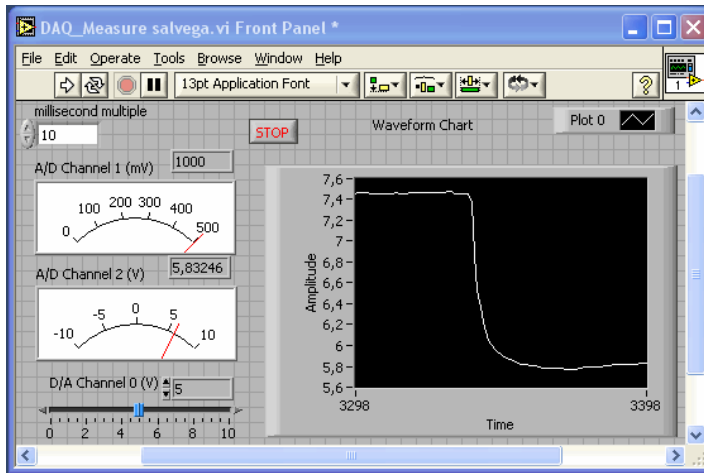


**Figure 2.6.** Front panel of the virtual instrument controlling temperature

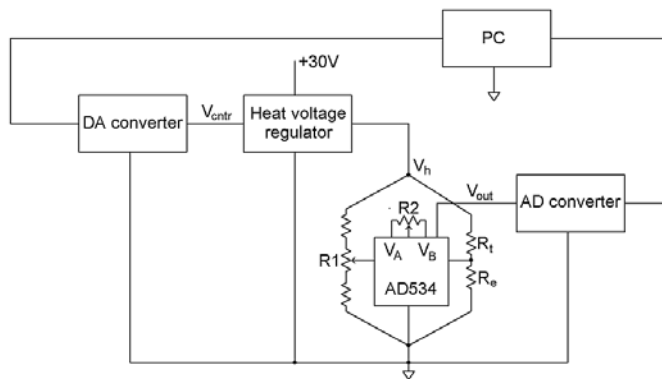


**Figure 2.7.** Temperature measuring and control unit

In order to measure relative changes in resistance, the controller device uses analogue-multiplication circuit AD534 in the percentage computation mode [48], i.e. two input signals  $V_A$  and  $V_B$  determine the output voltage

$$V_{out} = \frac{V_A - V_B}{V_B} V_{ref} G, \quad (4.1)$$

where  $V_{ref}$  is the internal reference voltage (10 V in this case),  $G$  is an amplification factor freely set by means of potentiometer  $R_2$  (to match the measurement range of the AD converter with the temperature range to be used – up to 200°C in case of polyethylene). The input voltage  $V_A$  is set by precision voltage divider  $R_1$  with a transfer function  $K$ , where  $V_A = V_h K$ .

$V_h$  is responsible for heating the transparent resistor film  $R_t$  in series system with a stable etalon resistor  $R_e$ . Resistance of the transparent heater film at a temperature  $T$  is

$$R_t = R_0[1 + \alpha(T - T_0)], \quad (2.2)$$

where  $\alpha$  is a constant characteristic to the ITO-layer and  $R_0$  is the resistance of the heater film at a temperature  $T_0$  to be chosen at the discretion of the user (e.g. in the lower part of the temperature range, i.e. at low  $V_h$ ). At  $T_0$  the bridge transition is equalized, so that  $V_{A0}=V_{B0}$  and  $V_{out}=0$ . The aim of equalizing is to have a reference point for temperature and to be able to work in the middle of the output range of the multiplier (which is  $\pm 10$  V), for the sake of reliability of results. The input signal  $V_B$  of AD534 depends on the resistance of the heater film, being

$$V_{B0} = V_h \left( \frac{R_e}{R_e + R_0} \right) \text{ at } T_0 \text{ and } V_B = V_h \left( \frac{R_e}{R_e + R_t} \right) \text{ at any temperature } T. \text{ After}$$

transforming equation (4.1) into  $\left( \frac{V_{B0}}{V_B} - 1 \right) G V_{ref} = V_{out}$  and substituting  $V_B$  and

$V_{B0}$ , the output voltage is expressed as

$$V_{out} = \left( V_h \left( \frac{R_e}{R_e + R_0} \right) / V_h \left( \frac{R_e}{R_e + R_t} \right) - 1 \right) G V_{ref} \text{ or more simply}$$

$$V_{out} = \left( \frac{R_e + R_t}{R_e + R_0} - 1 \right) G V_{ref}. \text{ After inserting } R_t \text{ from (2.2) and some more}$$

transformations the output voltage  $V_{out} = \frac{R_0 \alpha (T - T_0)}{R_e + R_0} G V_{ref}$ . So, as  $\alpha$ ,  $R_e$ ,  $R_0$  and

$V_{ref}$  are constants,  $V_{out}$  is proportional to the temperature difference from the equalization point.

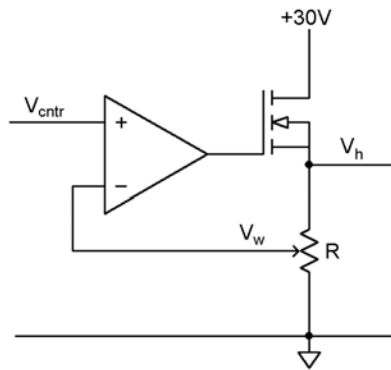


**Figure 2.8.** Heating voltage regulator

The heating voltage regulator (Figure 2.8) is connected to an external power supply, in the current case  $V = +30\text{ V}$ , and controlled by the output voltage of a PC-based DA converter. The control voltage  $V_{\text{ctr}}$  is compared to the voltage  $V_w$  from the wiper of potentiometer R, which is a part of the heating voltage  $V_h$ . The output of the operational amplifier  $V_G$  is connected to the gate of the power transistor, thereby changing the current of the transistor. If  $V_{\text{ctr}} > V_w$ , the output voltage of the amplifier changes to the positive direction, thus increasing the current of the transistor and the growth of  $V_h$  until  $V_{\text{ctr}} = V_w$ . If  $V_{\text{ctr}} < V_w$ , the current of the transistor decreases until  $V_{\text{ctr}} = V_w$ .

The output voltage of the controller needs calibration with every particular resistor sensor and cooling mode, calibration is done by means of a K-type thermocouple at a slow heating and cooling rate (1 min of stabilization time for every 5 K), a touch of heat conductive grease is applied to the thermocouple end for more stable signal.

The output signal for heating voltage values of 7,8 V and 5,4 V was registered at 10 ms intervals, characteristic time constant  $\tau$  was calculated from the slope of the logarithmic plot, signal from a small K-type thermocouple was registered for comparison.

## 2.5. Thermodynamic model of glass substrate

Given the use of a thin coated glass as the heater and temperature sensor, calculations had to be made to estimate how thick a glass substrate one can theoretically afford. If the heat capacity of the polymer sample and the heater film are assumed to be negligible compared to the substrate glass, their contact with each other very good (meaning equal temperature of the three) and the cooling capacity of the flowing liquid to be infinite, so that the temperature of the cooled side of the glass remains constant, a model can be used describing the temperature gradient of a homogeneous layer, one surface of which having a constant temperature, the other being thermally isolated [49]. Initially, when both sides of the glass have constant temperature, the gradient is even (linear). When the heating power changes, temperature in the glass starts to change and the gradient is described by:

$$T(x,t) = T_0 + \sum_{k=0}^{\infty} \frac{8(-1)^k (T_m - T_0)}{\pi^2 (2k+1)^2} e^{-\left[\frac{\pi(2k+1)}{2d}\right]^2 \frac{\kappa t}{\rho c}} \sin\left[\frac{\pi(2k+1)x}{2d}\right]$$

A graphical expression of the temperature gradient through the substrate glass is depicted in Figure 2.9.

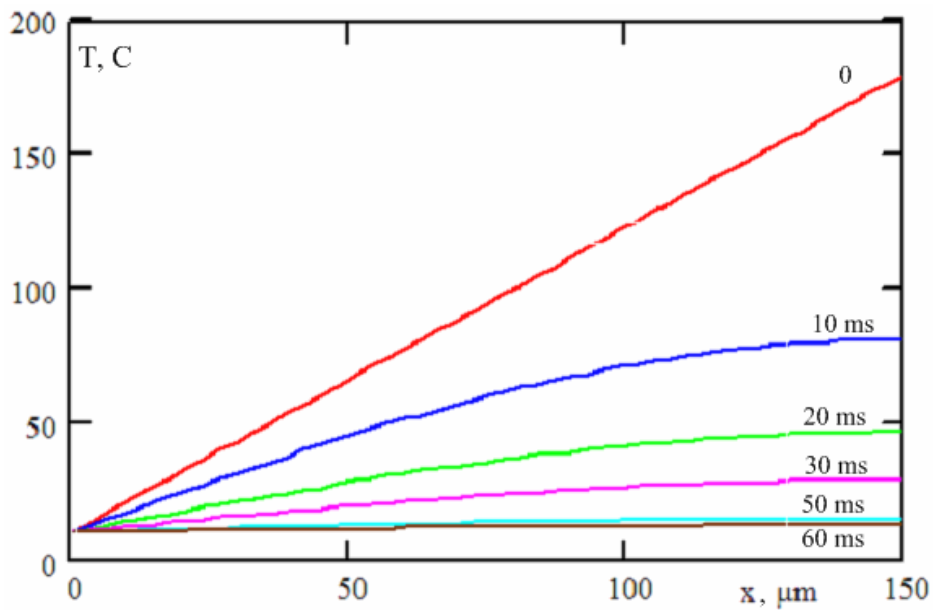


**Figure 2.9.** Temperature gradient in the glass (axial section) every 10 ms (descending order) after switching off the heating

Temperature change on the hot side of the glass is presented in Figure 2.10.

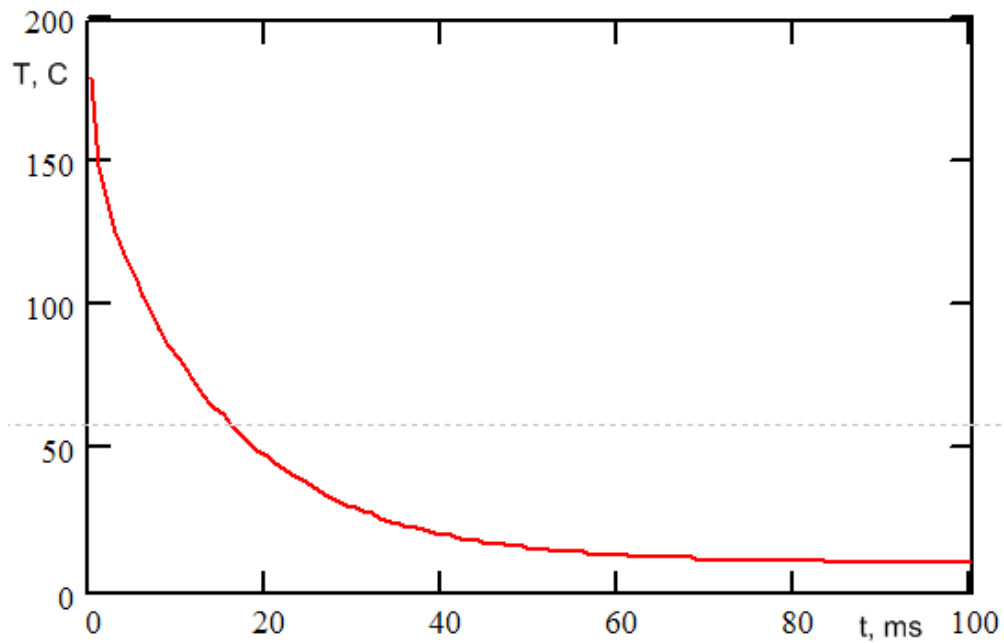


**Figure 2.10.** Cooling curve at the hot side of the glass ( $x=d$ )

In the logarithmic scale (Figure 2.11) it appears straight, except the very beginning.

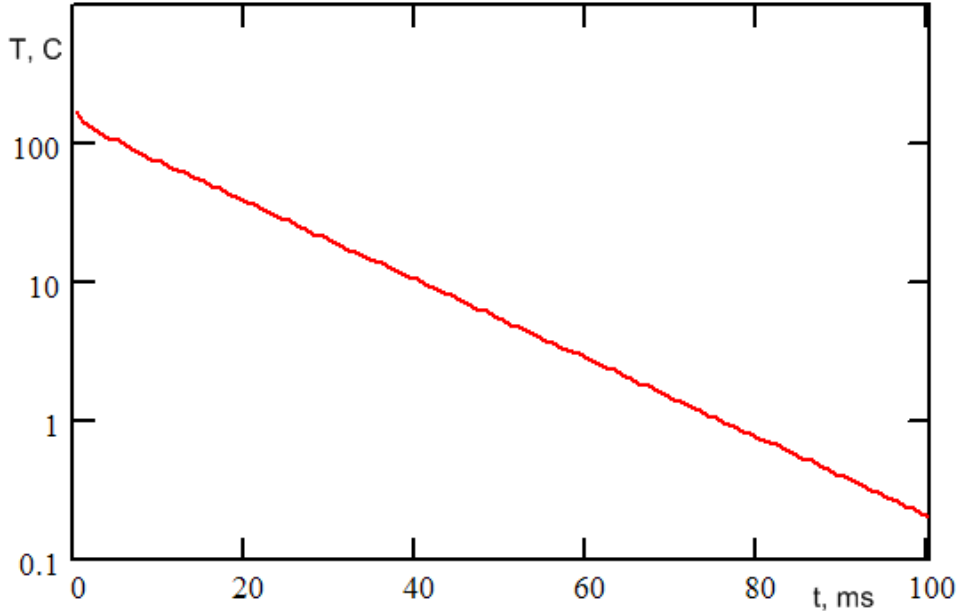


**Figure 2.11.** Logarithmic cooling curve at the hot side of the glass ( $x=d$ )

This means that prevailing is the largest member of the series ( $k=0$ ) and the spatial (sinusoid) component falls off, because, where  $x=d$ , its value is 1, leaving only the temporal dependence (i.e. exponential).

$$T(x, t) = T_0 + \frac{8(T_m - T_0)}{\pi^2} e^{-\left(\frac{\pi}{2d}\right)^2 \frac{\kappa t}{\rho c}}$$

The parameters in the exponent (its reciprocal) can be combined into the characteristic time constant of cooling  $\tau = \frac{4d^2 \rho c}{\pi^2 \kappa}$ . As roughly  $8/\pi^2 \approx 1$ , the resulting formula is quite convenient for practical calculations

$$(T - T_0) = (T_m - T_0) e^{-\frac{t}{\tau}} \text{ or in the logarithmic form } \ln \frac{(T - T_0)}{(T_m - T_0)} = -\frac{t}{\tau}.$$

Thus, the physical meaning of  $\tau$  is the time during which temperature difference decreases  $e=2.7182\dots$  times. The explicit expressions for temperature

$$T(t) = T_0 + (T_m - T_0) e^{-\frac{t}{\tau}} \text{ and for time } t = -\ln \frac{\tau(T - T_0)}{(T_m - T_0)}$$

enable one to make theoretical estimations on the heater temperature in a given time from switching off the heating and, beforehand, on how long it takes for the heater to cool from the pre-melting temperature down to a desired temperature of isothermal analysis.

### 3. RESULTS AND DISCUSSION

#### 3.1. Applicability of diverse methods – CNC vs HS PLM (II)

The study made on a pair of materials by two different methods, CNC and HS PLM, as described in 2.1, yielded data on linear growth rate of crystals depending on temperature in two separate temperature intervals (Figure 3.1). In case of CNC, the temperature vs time curves (Figure 3.2) were used for calculating the crystallization rate as described in Figure 2.1. With HS PLM, the resulting sigmoid-shape isotherms – light intensity (proportional to the number of light pixels) vs time, were differentiated and the reciprocal of time to the maximum growth moment served as a measure of crystallization rate. The data from the two different experiments fit into the same logarithmic extrapolation lines (Figure 3.1).

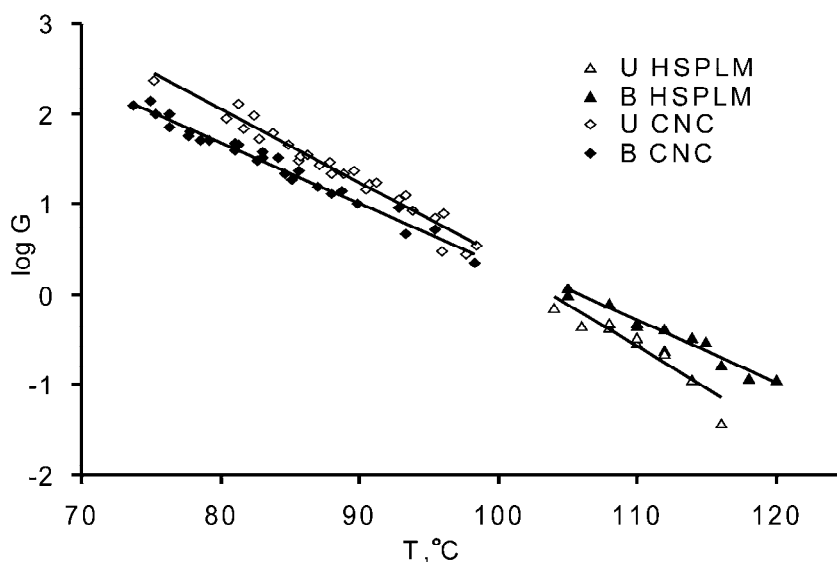


**Figure 3.1.** Crystallization rate  $G$  of two materials with different structural homogeneity at high and very high supercooling (by HS PLM and CNC respectively)

When moving down from the equilibrium melting temperature towards higher supercooling, the isothermal crystallization rate increases with the degree of supercooling, as could be expected. The fact that unimodal materials (with homogeneous MMD and SCBD) crystallize slower than bimodal materials (having heterogeneous distributions and larger proportion of long ethylene sequences) at a similar average molar mass and branching content [50-52], proved to be valid in this study at temperatures above 100°C. But at very high supercooling the materials revealed an unexpected behaviour. Below 100°C the unimodal material had a higher crystallization rate than the bimodal one, although the bimodal material has

certainly broader MMD and higher content of long ethylene sequences than the unimodal one, implying a gradual change of crystallization mechanism, e.g. inclusion of branches in the crystal. The logarithmic interpolation lines of the uni- and bimodal materials have a crossover point at approximately 100°C.

This study also demonstrates the limits of applicability of these two techniques in terms of temperature of isothermal analysis – results obtained by the gas cooled hot-stage are not reliable below 105-106°C, because crystallization starts before temperature stabilizes, but, the CNC method (however fast the cooling) is not applicable above 95-98°C (the crystallization peak becomes so flat that it is difficult to distinguish it from the base line). So there is a gap to be filled by a reasonably fast and sensitive instrument.

On the other hand, looking into the CNC cooling curves – no matter how fast is the pseudolinear cooling rate in the beginning (a fragment is magnified in Figure 3.2) or how short the characteristic time constant of free cooling (Figure 3.3.) – if the cooling medium is of the same temperature as the set-point, reaching it takes too long a time, e.g. 100 to 300 ms (theoretically infinite). A more expedient way is to keep the ambient cold and compensate the cooling gradually.

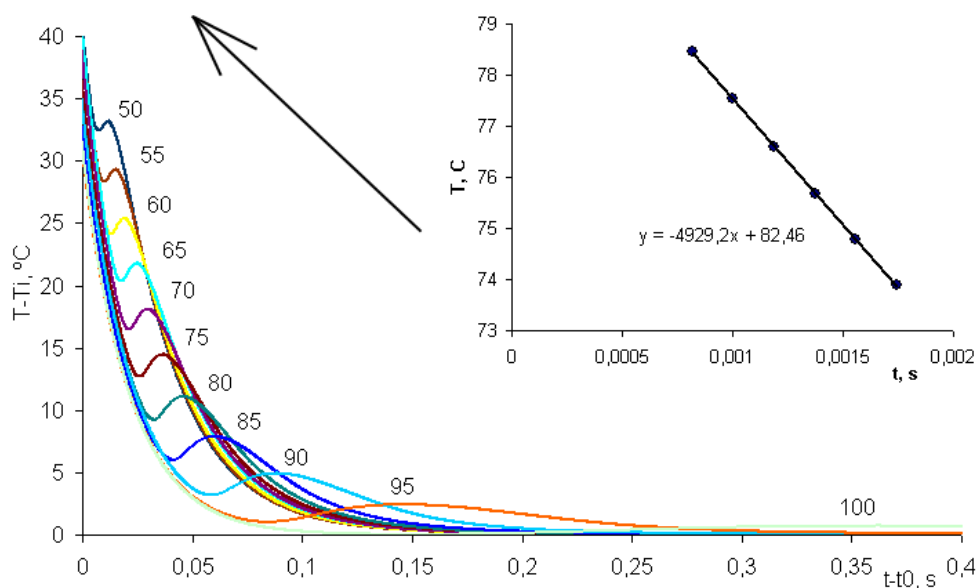


**Figure 3.2.** Examples of thermal curves by CNC – superposition of free cooling and crystallization exotherms, first 2 ms of free cooling magnified (insertion), revealing a pseudolinear scanning rate of 4929 K/s

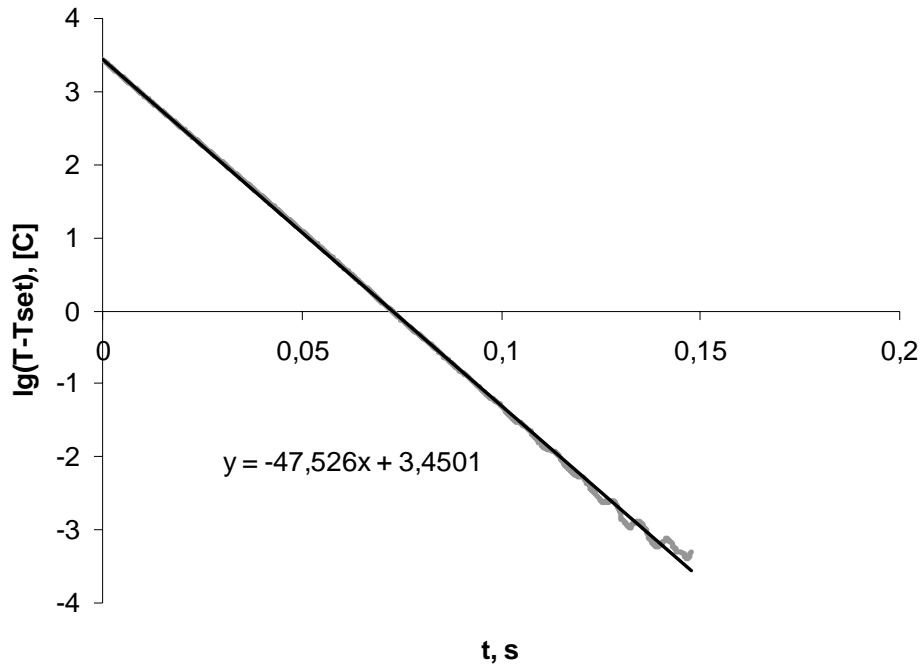


**Figure 3.3.** Calculation of  $\tau$  for the CNC device:  $\tau = 1/47,5 = 0,021$  s or 21 ms

### 3.2. Gas cooling

Crystal growth curves by light intensity (proportional to the number of light pixels, Figure 3.4) and temperature dependence of calculated growth rate (Figure 3.5) obtained on the first, electrically heated and gas-cooled device show that LLDPE crystallization analysis at 103°C is yet feasible. In [36] the lowest feasible temperature for LMM PE analysis is reported to be 109°C. The experiments in this work (as described in 2.1 and results in 3.1) made on the same gas-heated/cooled hot-stage showed that the lowest isothermal analysis temperature the device reached before discernible crystallization of LLD PE started, was 105°C (the difference is well explained by the difference in the materials' SCB and MM). Altogether it can be said that, although direct heating and temperature sensing has expanded the applicability of the hot stage by roughly 5 K to lower supercooling, the effect was still not worth the effort – gas cooling is not efficient enough. Besides, every time the gas flow is changed, new PID tuning is necessary, which is time consuming. Gas flow is also easily disturbed by occasional air movements and, thus, unstable. Neither would have been stable the cooling by evaporation of a volatile liquid.

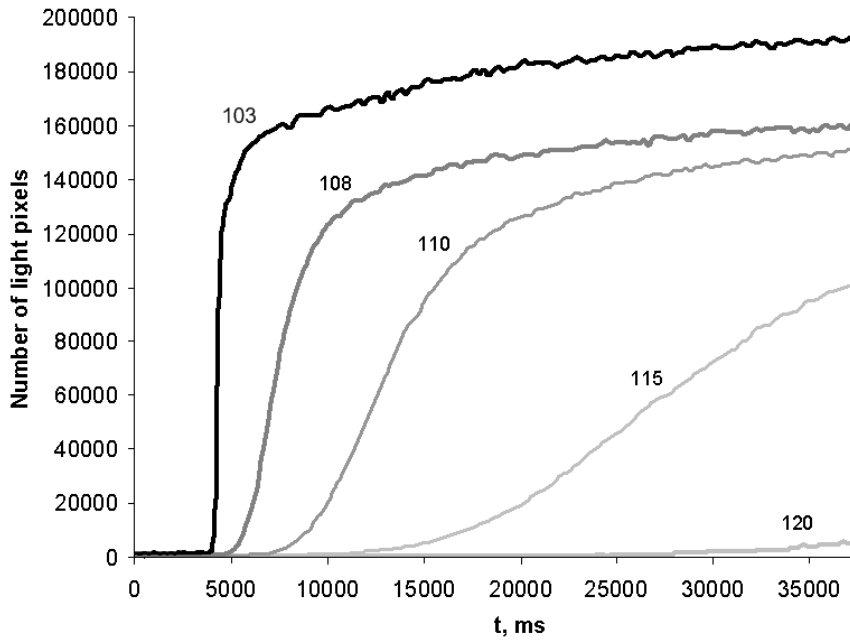


Figure 3.4. Growth of crystals (based on the number of light pixels as described in 2.1)

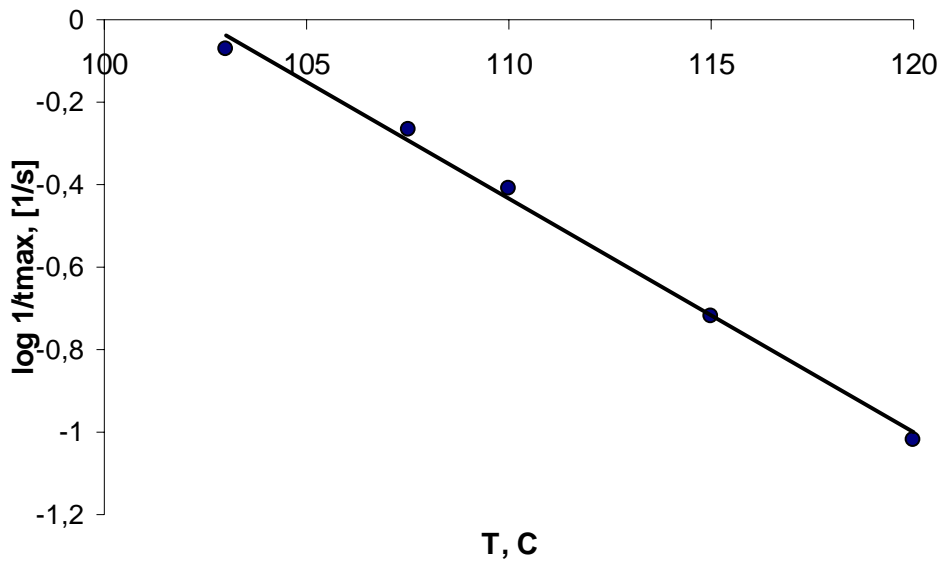


Figure 3.5. Growth rate (reciprocal of time to maximum growth rate)

### 3.3 Transparent heater – gold and other metals *versus* ITO

During crystallization experiments on the gold film based hot-stage a drift of the calibration curve was observed, which can be explained by the change of morphology of the thin gold film during heating, bringing about a change in resistance. The thin gold layer also turned out very soft and was easily scratched, so reuse of the same gilded glass for another sample would at best require a new calibration. Thus, other transparent conductive materials were considered. Efforts were made to deposit nickel by thermal evaporation, but the eventual result was not very transparent and it peeled off from the glass, which could be explained by the stiffness of nickel or too different expansion coefficients. The fine copper spirals were mechanically durable but burned out easily. A thin  $\text{Al}_2\text{O}_3$  layer helps to reduce the gradual oxidation of the copper layer – the drift of calibration plots is only marginal, and although the transparency is not as good as with ITO and the  $\text{Al}_2\text{O}_3$  layer may also worsen thermal contact, it is worth considering as an option. (The tested sample broke at  $120^\circ\text{C}$  due to substrate thickness, 0.5mm.) ITO layer showed good transparency (visually compared), good mechanical endurance and stability of resistance (temperature plot, Figure 3.6, is well reproduced). Its somewhat weaker temperature dependence of resistance was made up for by the mentioned advantages and the amplifying capability of the electronics unit.

### 3.4. Thermal tests on ITO-coated glasses

ITO-coated glass samples of 1mm and 0.4 mm thickness were broken at testing (as in 2.4) already between temperatures  $100\text{-}130^\circ\text{C}$  at slow heating ( $10\text{ K/min}$ ). The 0.175 mm thick glass passed thermal shock test – no breakage below  $200^\circ\text{C}$ . Resistance *vs* temperature was measured as described in 2.3, the plot in Figure 3.6 shows feasibility of temperature measurements by resistance of ITO-film. Heating test of the system with a 24 V power supply and flowing water yielded a maximum temperature of  $130^\circ\text{C}$ , as the heating voltage did not rise above 14 V (10 V is used by the controller). 30 V power unit enables one to raise the temperature to  $180^\circ\text{C}$ .

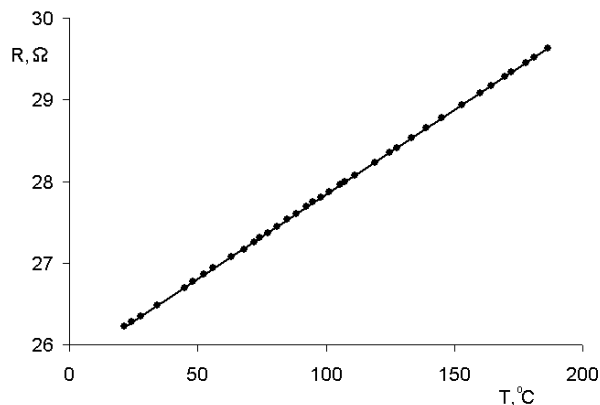


Figure 3.6. Temperature dependence of resistance of an ITO-coated glass sample

### 3.5. Results of modelling the substrate glass

Using the expressions of time and temperature obtained in 2.5, inserting the parameters of glass and a typical value for the initial (heater) temperature:

$\kappa=1.1$  W/(m·°C) (heat conductivity of glass);

$\rho=2.5$  g/cm<sup>3</sup> (density of glass);

$c=840$  J/(kg·°C) (heat capacity of glass);

$T_m=180^\circ\text{C}$  (heater temperature, suitable for pre-melting a number of polymers);

and varying the values for glass thickness among available standard ones (0.15mm, 0.175mm, 0.4mm, 0.7mm) and several feasible values for the cooling temperature (from the most convenient, room temperature down to  $T_0=-50^\circ\text{C}$ ), an array of calculation results is obtained and presented in Table 2.

Table 2. Time to analysis temperature at various glass thickness and cooling liquid temperature (theoretical)

		$T_{\text{cool}} = 20^\circ\text{C}$	$T_{\text{cool}} = 10^\circ\text{C}$	$T_{\text{cool}} = 0^\circ\text{C}$	$T_{\text{cool}} = -50^\circ\text{C}$
Glass thickness 0.15 mm ( $\tau=19$ ms)	time (ms) to 100°C	13	12	11	8
	time (ms) to 80°C	19	17	15	11
	time (ms) to 60°C	36	23	21	14
	$T, ^\circ\text{C}$ at 10 ms	115	110	106	86
	$T, ^\circ\text{C}$ at 100 ms	21	11	1	-49
Glass thickness 0.175 mm ( $\tau=26$ ms)	time (ms) to 100°C	18	17	15	11
	time (ms) to 80°C	26	23	21	15
	time (ms) to 60°C	36	32	29	19
	$T, ^\circ\text{C}$ at 10 ms	98	93	88	62
	$T, ^\circ\text{C}$ at 100 ms	20	10	0	-50
$\tau=51$ ms (experim.)	time (ms) to 80°C	51	46	42	29
	time (ms) to 60°C	71	63	57	38
Glass thickness 0.4 mm ( $\tau = 136$ ms)	time (ms) to 100°C	94	86	80	58
	time (ms) to 80°C	133	121	110	78
	time (ms) to 60°C	189	166	149	100
	$T, ^\circ\text{C}$ at 10 ms	169	168	167	164
	$T, ^\circ\text{C}$ at 100 ms	97	91	86	60
	$T, ^\circ\text{C}$ at 200 ms	57	49	41	3
Glass thickness 0.7 mm ( $\tau = 417$ ms)	time (ms) to 100°C	289	265	245	178
	time (ms) to 80°C	409	370	338	238
	time (ms) to 60°C	578	510	458	308
	$T, ^\circ\text{C}$ at 10 ms	176	176	176	175
	$T, ^\circ\text{C}$ at 100 ms	146	144	142	131
	$T, ^\circ\text{C}$ at 200 ms	119	115	111	92
	$T, ^\circ\text{C}$ at 400 ms	81	75	69	38

Considering the time to a given analysis temperature, one can calculate a pseudolinear cooling rate, dividing the temperature change from the pre-melting temperature to the analysis temperature by the respective time interval (results shown in Table 3).

Table 3. Theoretical pseudolinear temperature scan rates  $\beta$  for a set of glass thickness, analysis temperature and cooling liquid temperature values

		$T_{cool}$ 20°C	$T_{cool}$ 10°C	$T_{cool}$ 0°C	$T_{cool}$ -50°C
<b>Glass thickness</b> <b>0.175 mm</b> <b>(<math>\tau = 26ms</math>)</b>	$\beta$ to 100°C, K/s	4439	4838	5235	7198
	$\beta$ to 80°C, K/s	3921	4335	4743	6741
	$\beta$ to 60°C, K/s	3329	3771	4201	6257
<b><math>\tau = 51ms</math></b> <b>(experimental)</b>	$\beta$ to 80°C, K/s	1960	2174	2381	3448
	$\beta$ to 60°C, K/s	1690	1905	2105	3158
<b>Glass thickness</b> <b>0.4 mm</b> <b>(<math>\tau = 99 ms</math>)</b>	$\beta$ to 100°C, K/s	849	925	1001	1376
	$\beta$ to 80°C, K/s	750	829	907	1289
	$\beta$ to 60°C, K/s	636	721	803	1196
<b>Glass thickness</b> <b>0.7 mm</b> <b>(<math>\tau = 303ms</math>)</b>	$\beta$ to 100°C, K/s	277	302	326	449
	$\beta$ to 80°C, K/s	244	270	296	420
	$\beta$ to 60°C, K/s	208	235	262	390

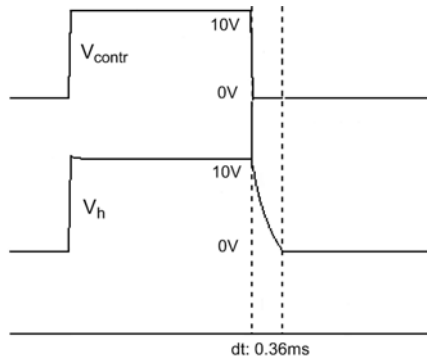
Comparing the scan rate estimations (Table 3) with the critical cooling rates calculated by formula 1.2 in 1.1.3 (Table 4), one can deduce that, in theory, substrate glass thickness 0.175 mm would allow isothermal crystallization studies of PE down to 70°C, and when lowering the cooling temperature to -50°C, even at 60°C (that is the temperature of maximum rate of crystal growth for PE (as explained in 1.1.3, Figure 1.1)). The real system, yielding a  $\tau = 51.5$  ms, would also allow PE analysis at 80°C.

Table 4. Critical cooling rates for various isothermal analysis temperatures for PE

T, °C	$q_{crit}$ , K/s
90	100
80	1000
70	2300
60	3000

### 3.6. Parameters of the controller

An important parameter of the voltage regulator is its speed of regulating the heating voltage  $V_h$ , for the sake of fast temperature changes of the polymer sample on the heater.



**Figure 3.7.** Response of the heating voltage to the control voltage

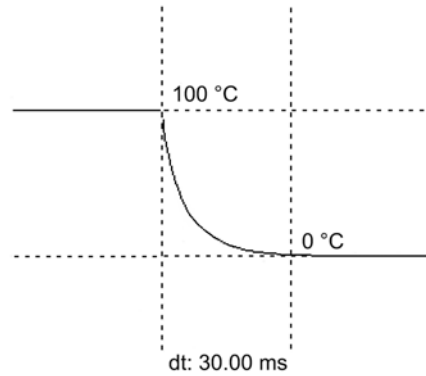


**Figure 3.8.** Output voltage of the multiplier vs time at a pulse change of  $R_0$ , equivalent to a temperature change of  $100^\circ\text{C}$

Figure 3.7 demonstrates the fast response of the heating voltage  $V_h$  to the pulsed control voltage  $V_{\text{ctr}}$  – the time lag is only 0.30 ms. The time diagram in Figure 3.8 describes the decrease of the output voltage  $V_{\text{out}}$  of the bridge, when in place of the glass-based film heater an effective resistor wire was used, the resistance of which was sharply changed, imitating the change in the resistance of the ITO-film at a temperature change of 100 K. This demonstrates the ability of the bridge to register

temperature changes up to  $\frac{100\text{K}}{30 \times 10^{-3}\text{s}} \approx 3000\text{K/s}$ .

According to the parameters of the switch, the output voltage is 1 V at the maximum value of the amplification factor, if  $V_A$  and  $V_B$  differ for 0.1 %. An example of temperature calibration is shown in Figure 3.10. Although sensitivity can be regulated in order to match the measurement range of the AD converter with the temperature range to be used, it is not expedient to use the whole range, medium sensitivity yields better stability of the signal. Only a quarter of the output range ( $\pm 10\text{ V}$ ) is used.

### 3.7. Output signal, temperature calibration

Output signal of the ITO-water hot-stage system recorded at sharp changes of control voltage at intervals of 10 ms is shown in Figure 3.9 together with the thermocouple signal.

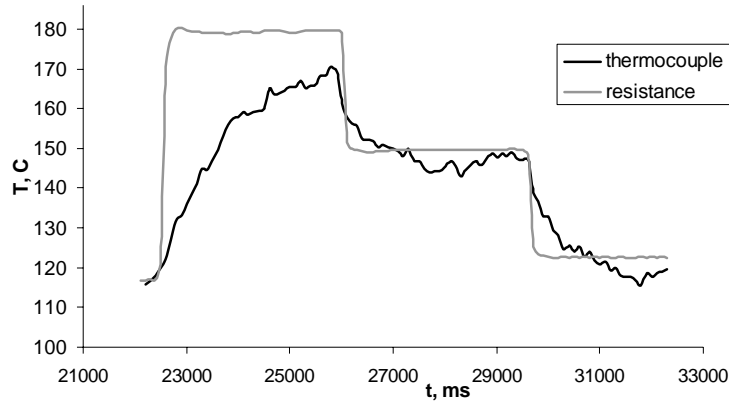


**Figure 3.9.** Temperature signals by resistance of ITO film and by thermocouple

The applied rate  $\sim 2.5$  s for 30 K temperature difference is too high even for a thin flat wire thermocouple. Temperature by resistance is slightly unstable at the pre-melting temperature, perhaps this can be explained by the strong cooling effect of laboratory air at this large temperature difference.

Temperature calibration plot (Figure 3.10) of the ITO-water hot stage with the temperature measurement and control unit shows that the temperature dependence of the output signal of the system is linear between 25 and 180°C with a good correlation coefficient and, thus, fit for controlling of crystallization analysis temperature. The sensitivity can be freely set.

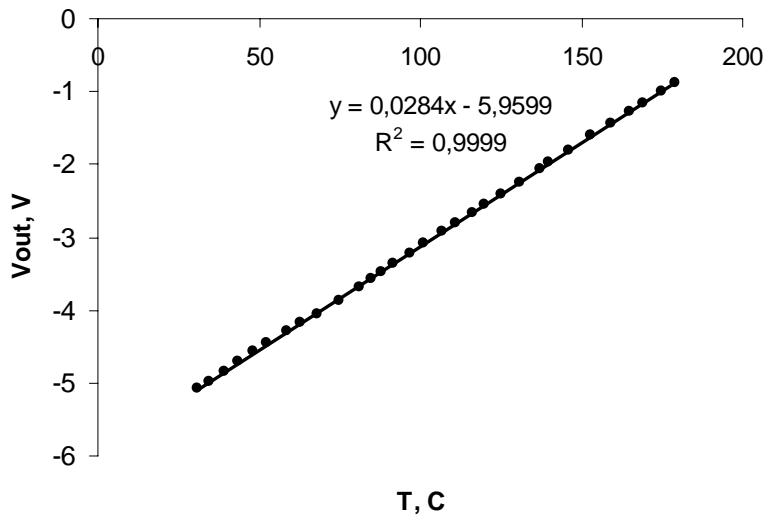


**Figure 3.10.** An example of temperature calibration by K-type thermocouple

Attempts were made to calibrate the temperature of an ITO-glass by an IR-sensor, but this method gave distorted results. Results of simultaneous measurement by the IR-sensor and the thermocouple in Figure 3.11 reveal a difference up to 15°C at medium temperatures, implying that in case of glossy surfaces application of an IR sensor is complicated due to disturbing reflection.

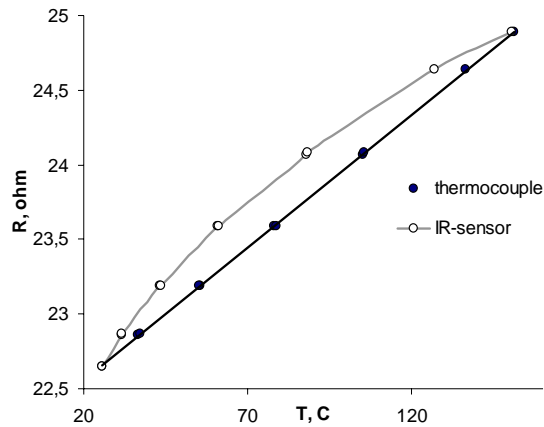


**Figure 3.11.** Resistance of ITO-film vs temperature by K-type thermocouple and IR-sensor

### 3.8. Experimental time constants vs theoretical

Comparison of cooling curves from various types of hot stages show that the cooling capacity of my first prototype (grey line in Figure 3.12) is not considerably better than that of the gas-cooled and – heated hot stage [36] (the continuous black line).

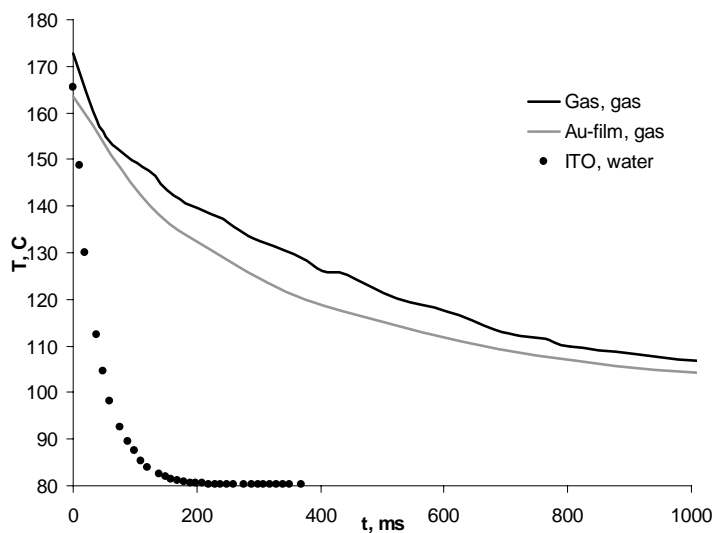


**Figure 3.12.** Cooling curves of various hot stages

And logarithmic plots (Figure 3.13) show the similarity even better.

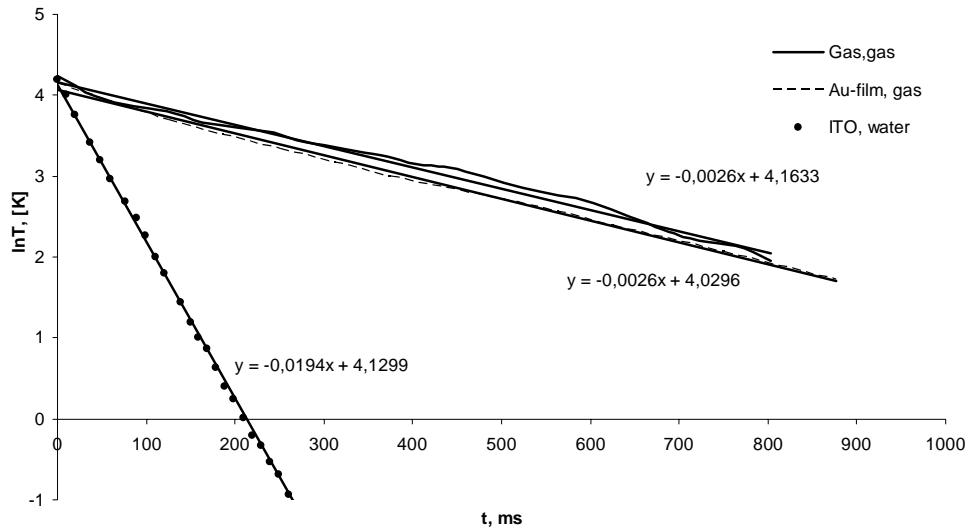


**Figure 3.13.** Cooling curves in a logarithmic scale for various hot stages

Time constants (from the definition formula in 2.5 – negative reciprocal of the slope of the logarithmic temperature-time plot) for the two gas-cooled types appeared equal ( $\tau=167$  ms). Time constant for the ITO-water type being considerably longer than theoretical (51.5 vs 26 ms) could be explained by the trapezoid shape of the gold contact layer (Figure 2.4), which allows certain heat production on the periphery (including the flange), which during the cooling period warms the central measurement area (“backward heat transfer”). Another factor of the peripheral warming is the heat conductivity of the contact layer.

The effective stabilization period of temperature – approximately 0.2 s for the ITO-water type hot-stage (black dots in Figure 3.11), yields a pseudolinear cooling rate of  $100/0,2=500$  K/s, which is 30 times faster than the gas-cooled type and 200 times faster than the commercial hot-stages. Still it is longer than it could possibly be, because the heating voltage was changed by rectangular steps. Since the current controller design uses the heating voltage for one shoulder of the bridge transition (i.e. for temperature measurement), it was not possible to record the cooling curve with the heating voltage switched off (i.e. heating voltage switched to 0 V). Steady heating raises the free exponential cooling curve, just as if the cooling liquid temperature were that of the set-point, causing an infinite prolongation of the time to the set-point (Figure 3.11). The calculation model introduced in 2.5 is not applicable in such a situation where the set-point and cooling temperature are equal – it would lead to dividing by zero.

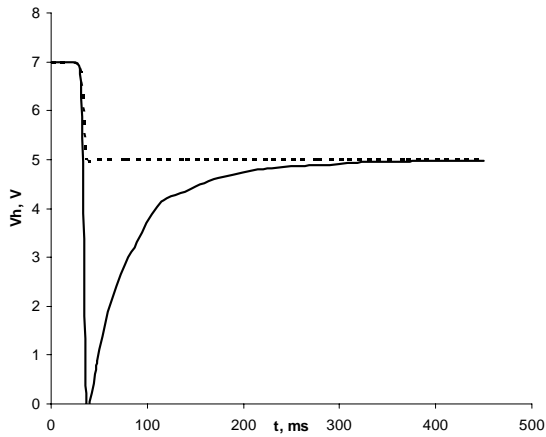


**Figure 3.14.** A heating power program (bold line) to gradually compensate free cooling and meet the temperature at the desired level early

Simulating a situation where the heating is switched off, by inserting the experimentally obtained  $\tau = 51.5$  ms into the expression of time (in 2.5), yields the time to  $80^\circ\text{C}$  is 51 ms and the time to  $60^\circ\text{C}$  is 71 ms. When dividing the temperature intervals by the respective time intervals, the pseudolinear cooling rates would be  $100\text{ K}/0.051\text{ s} = 1960\text{ K/s}$  and  $120\text{ K}/0.071\text{ s} = 1690\text{ K/s}$ . Such rates can be attained with this real system, if the heating is programmed to be gradually growing from zero to the set-point value.

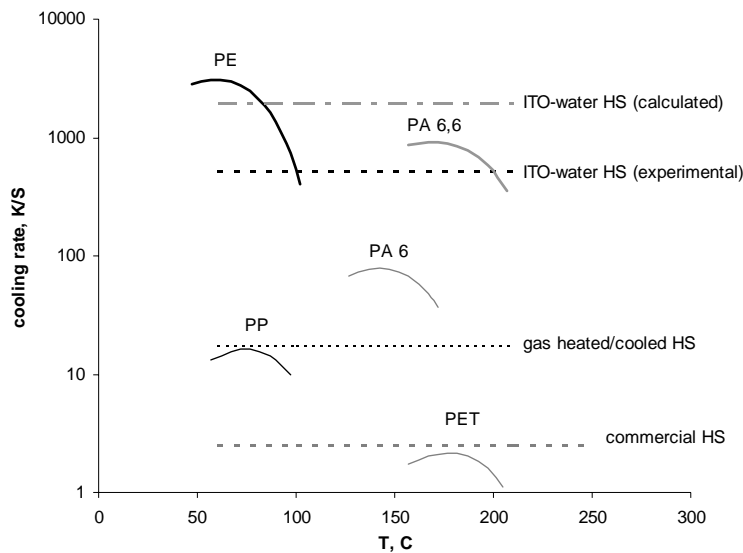


**Figure 3.15.** Calculated critical cooling rates to precede 99% of crystallization around temperatures of maximum crystal growth rate for a variety of materials. Maximum or effective cooling rates of a variety of hot stages (horizontal lines)

When compared to the critical cooling rates calculated by formula 1.2, it means that PE crystallization analysis at 80°C is feasible. This is at least 25 K towards higher supercooling compared to the gas heated and cooled hot-stage (as explained in 3.1 and 3.2). Graphical illustration of the situation is presented in Figure 3.15. Calculations predict that the new type hot-stage can exceed the crystal growth maximum for polyamide 6,6, although literature sources [6] report a discernible discrepancy (underestimation) between calculated and experimental data when polyamide is concerned, possibly due to the polarity of groups.

#### 4. CONCLUSIONS

1. In a comparative study by chip nanocalorimetry and hot-stage polarization light microscopy a qualitative difference was discovered in the crystallization behaviour of materials at high supercooling compared to moderate, implying a change of crystallization mechanism – inclusion of branches in the *lamella* at high supercooling that are normally excluded (at moderate supercooling).

2. Based on the new concept with lesser tools of less mass, better transparency, more efficient and stable cooling, judicious control unit and calculated heating pattern, the novel design for a hot-stage with electrically heated ITO-film on a 0.175 mm glass substrate and direct room-temperature flowing water cooling ensures fast controlled cooling of the sample:

1. A real cooling rate of 500 K/s was attained, 30 times exceeding that of the existing microscopy hot-stages;
2. The attained cooling rate can be at least doubled by an exponentially developing heating pattern and further raised by lowering the cooling water temperature;
3. Calculations show that the novel hot-stage design and methodology broaden the applicability of optical study methods of fast crystallization of polymers (polyethylene beforehand) for more than 25 K towards larger supercooling;
4. In contrast to chip nanocalorimetry, the novel robust design of hot-stage makes it accessible for routine measurements, maintaining the cooling performance comparable to the aforementioned chip nanocalorimetry and enabling morphology studies.

## REFERENCES

- [1] Eisele, U. Introduction to Polymer Physics. Springer-Verlag Berlin Heidelberg New York, 1990.
- [2] Van Krevelen, D. V. Crystallinity of polymers and the means to influence the crystallization process. *Chimia*, 1978, 32, 8, 279.
- [3] Gedde, U. W. Polymer physics. London: Chapman & Hall, 1995.
- [4] Bassett, D. C. On spherulitic growth and cellulation in polymers. A unified context. *Polym. J.*, 1999, 31, 759-764.
- [5] Vaughan, A. S., Bassett, D. C. Crystallization and morphology. In: Allen, G., editor. Comprehensive polymer science, vol. 2. New York: Pergamon, 1989.
- [6] Mandelkern, L. The structure of crystalline polymers. *Acc. Chem. Res.*, 1990, 23, 380-386.
- [7] Bassett, D. C., Hodge, A. M., Olley, R. H. Lamellar morphologies in melt-crystallized polyethylene. *Faraday Discussions R. Soc. Chem.*, 1979, 68, 216-224.
- [8] Rego, J. M., Gedde, U. W. Morphology of binary linear polyethylene blends. *Polymer*, 1988, 29 1037-1044.
- [9] Gedde, U. W., Jansson, J. F., Liljenström, G., Eklund, S., Holding, S. R., Wang, P. L., Werner, P.E. Molecular structure, crystallization behaviour, and morphology of fractions obtained from an extrusion grade high-density polyethylene. *Polym. Eng. Sci.*, 1988, 28, 1289-1303.
- [10] Mandelkern, L., Alamo, R. G., Kennedy, M. A. Interphase thickness of linear polyethylene. *Macromolecules*, 1990, 23, 4721-4723.
- [11] Peacock, A. J. Handbook of polyethylene. New York: Marcel Dekker, 2000.
- [12] Fatou, J. G., Marco, C., Mandelkern, L. The crystallization kinetics of low-molecular-weight polyethylene fractions. *Polymer*, 1990, 31, 890-898.
- [13] Arnal, M. L., Balsamo, V., Ronca, G., Sanchez, A., Müller, A. J., Cañizales, E., Urbina de Navarro, C. Applications of successive self-nucleation and annealing (SSA) to polymer characterization. *J. Therm. Anal. Calorimetry*, 2000, 59, 451-470.
- [14] Hu, S. R., Kyu, T., Stein, R. S. Characterization and properties of polyethylene blends I. Linear low-density polyethylene with high-density polyethylene. *J. Polym. Sci. Part B: Polym. Phys.*, 1987, 25, 71-87.
- [15] Puig, C. C., Hill, M. J., Odell, J. A. Absence of isothermal thickening for a blend of linear and branched polyethylene. *Polymer*, 1993, 34, 3402-3407.
- [16] Alamo, R. G., Mandelkern, L. The crystallization behavior of random copolymers of ethylene. *Thermochimica Acta*, 1994, 238, 155-201.
- [17] Wunderlich, B. *Macromolecular physics*, vol. 3. New York: Academic Press, 1980.
- [18] Fatou, J. G., Mandelkern, L. The effect of molecular weight on the melting temperature and fusion of polyethylene. *J. Phys. Chem.*, 1965, 69, 417-428.
- [19] Di Lorenzo, M. L., Silvestre, C. Non-isothermal crystallization of polymers. *Prog. Polym. Sci.*, 1999, 24, 917-950.

- [20] Ergoz, E., Fatou, J. G., Mandelkern, L. Molecular weight dependence of the crystallization kinetics of linear polyethylene. I. Experimental results. *Macromolecules*, 1972, 5, 147-157.
- [21] Becker, R., Döring, W. The kinetic treatment of nuclear formation in supersaturated vapors. *Annalen der Physik*, 1935, 24, 719-52.
- [22] Mandelkern, L., Jain, N. L., Kim, H.-G. Temperature dependence of the growth rate of spherulites. *J. Polym. Sci., Polymer Physics*, 1968, 6, 1, 165-80.
- [23] Gandica, A., Magill, J. H. Universal relation for the crystallization kinetics of polymeric materials. *Polymer*, 1972, 13, 12, 595-6.
- [24] Van Antwerpen, F., Van Krevelen, D. W. Influence of crystallization temperature, molecular weight, and additives on the crystallization kinetics of poly(ethylene terephthalate). *J. Polym. Sci.: Polym. Phys.*, 1972, 10, 12, 2423-35.
- [25] Supaphol, P., Spruiell, J. E. Nonisothermal bulk crystallization studies of high density polyethylene using light depolarizing microscopy. *J. Polym. Sci. Part B: Polym. Phys.*, 1998, 36, 681-692.
- [26] Chiu, F. C., Fu, Q., Hsieh, E. T. Molecular weight dependency of melt crystallization behavior and crystal morphology of low molecular weight linear polyethylene fractions. *J. Polym. Res.*, 1999, 6, 219-229.
- [27] Chiu, F. C., Fu, Q. Crystallization behavior and crystal morphology of HDPE – molecular weight dependence. *ANTEC*, 1999, 3770-3774.
- [28] Fatou, J. G., Marco, C., Mandelkern, L. The influence of molecular weight on the regime crystallization of linear polyethylene. *Polymer*, 1990, 31, 1685-1693.
- [29] Wagner, J., Phillips, P. J. The mechanism of crystallization of linear polyethylene, and its copolymers with octene, over a wide range of supercoolings. *Polymer*, 2001, 42, 8999-9013.
- [30] Hoffman, J. D., Miller, R. L. Test of the reptation concept: Crystal growth rate as a function of molecular weight in polyethylene crystallized from the melt. *Macromolecules*, 1988, 21, 3038-3051.
- [31] Maxfield, J., Mandelkern, L. Crystallinity, supermolecular structure, and thermodynamic properties of linear polyethylene fractions. *Macromolecules*, 1977, 10, 1141-1153.
- [32] Ratajski, E., Janeschitz-Kriegl, H. How to determine high growth speeds in polymer crystallization. *Colloid Polym. Sci.*, 1996, 274, 938-951.
- [33] Eder, G. Crystallization in polymer processing: Modelling and experimentation. In: Arkeryd L. et al. editors. Progress in industrial mathematics at ECMI 98. Stuttgart: B.G. Teubner, 1999.
- [34] Mathot, V. B. F., Poel, G. V., Pijpers T. F. J. Improving and speeding up the characterization of substances, materials and products: benefits and potentials of high-speed DSC. *Am. Lab.*, 2006, 38, 14, 21-25.
- [35] Linkam Data Sheet. [http://www.linkam.co.uk/index.php?page=shop.product\\_details&product\\_id=31&category\\_id=31](http://www.linkam.co.uk/index.php?page=shop.product_details&product_id=31&category_id=31).
- [36] Krumme, A. Measuring crystallization kinetics of high density polyethylene by improved hot-stage polarized light microscopy. *Polym. Test.*, 2004, 23, 29-34.
- [37] Perkin Elmer <http://las.perkinelmer.com/News/News+Details/03132006b.htm>

- [38] Ding, Z., Spruiell, J. E. An experimental method for studying nonisothermal crystallization of polymers at very high cooling rates. *J. Polym. Sci. Part B: Polym. Phys.*, 1996, 34, 2783-2804.
- [39] Stadlbauer, M., Eder, G., Janeschitz-Kriegl, H. Crystallization kinetics of two aliphatic polyketones. *Polymer*, 2001, 42, 3809-3816.
- [40] Brucato, V., De Santis, F., Giannattasio, A., Lamberti, G., Titomanlio, G. Crystallization During Fast Cooling Experiments, a Novel Apparatus for Real Time Monitoring. *Macromol. Symp.*, 2002, 185, 181-186.
- [41] Kwan, A. T., Efremov, M. Yu., Olson, E. A., Schiettekatte, F., Zhang, M., Geil, P. H., Allen, L. H.. Nanoscale Calorimetry of Isolated Polyethylene Single Crystals. *J. Polym. Sci. Part B: Polym. Phys.*, 2001, 39, 1237-1245.
- [42] Merzlyakov, M. Method of rapid ( $100\,000\text{ Ks}^{-1}$ ) controlled cooling of samples. *Thermochimica Acta*, 2006, 442, 52-60.
- [43] Winter, W., Höhne, W. H. Chip calorimeters for small samples. *Thermochimica Acta*, 2003, 403, 43-53.
- [44] Minakov, A., Wurm, A., Schick, C. Superheating in linear polymers studied by ultrafast nanocalorimetry. *Eur. Phys. J.*, 2007, 23, 43-53.
- [45] Minakov, A., Schick, C. Ultrafast thermal processing and nanocalorimetry at heating and cooling rates up to 1 MK/s. *Rev. Sci. Instr.*, 2007, 78, 073902.
- [46] Behrisch, R. (ed.). Sputtering by Particle bombardment. Springer, Berlin, 1981.
- [47] Jaeger, R. C. Film Deposition. *Introduction to Microelectronic Fabrication*. Upper Saddle River: Prentice Hall, 2002.
- [48] AD534 Data Sheet. [www.analog.com/static/imported-files/data\\_sheets/AD534.pdf](http://www.analog.com/static/imported-files/data_sheets/AD534.pdf)
- [49] Habermann, R.. Elementary applied partial differential equations. Prentice Hall, Englewood Cliffs, New Jersey, 1987.
- [50] Zhang, M., Lynch, D. T., Wanke, S. E. Effect of molecular structure distribution on melting and crystallization behavior of 1-butene/ethylene copolymers. *Polymer*, 2001, 42, 3067-3075.
- [51] Kim, M.-H., Phillips, P. J. Nonisothermal melting and crystallization studies of homogeneous ethylene/ $\alpha$ -olephin random copolymers. *J. Appl. Polym. Sci.*, 1998, 70, 1893-1905.
- [52] Wagner, J., Abu-Iqyas, S., Monar, K., Phillips, P. J. Crystallization of ethylene-octene copolymers at high cooling rates. *Polymer*, 1999, 40, 4717-4721.

## KOKKUVÕTE

### Metoodika ja seade kiirelt kristalluvate polümeeride optilisteks uuringuteks

Kristallisatsioon on termoplastsest polümeerist toote kujunemise võtmefaas – kas ja kuidas see toimub, kuna reaalses töötlemisprotsessides kasutatavatel madalatel temperatuuridel tekki metastabiilne morfoloogia (kristallide kuju ja suurus ning amorfse materjali osakaal) mõjutab oluliselt tema omadusi. Seega on uute omadustega modifitseeritud materjalide väljatöötamise seisukohast oluline simuleerida ja süstemaatiliselt uurida kristallisatsiooniprotsessi madalatel temperatuuridel (suurtel allajahutustel). Kõigist erineva keemilise koostise (laengute jaotuse) ja ahela geomeetriaga polümeerimaterjalidest, mis seeläbi oluliselt erinevad ka kristallumiskiiruse poolest, on polüetüleenil üks kõige järsemad kiiruse temperatuurisõltuvusi. Kõige laiemalt kasutatava ja samas lihtsaima struktuuriga polümeerina on teda sageli uuritud kui mudelit polümeerimaterjalide käitumise üldisemaks mõistmiseks, kuigi talle omane suur kristallumiskiirus komplitseerib uurimist madalamatel temperatuuridel, kus kiirus suureneb märkimisväärselt.

Kristallisatsiooni kui väga temperatuuritudliku protsessi uurimiseks on tarvis vahendit temperatuuri kiireks ja täpseks ning kontrollitud muutmiseks. Kaubanduslikult saadaolevad kuumalused, mille küttekeha ja ka jahuti on traditsiooniliselt monoliitse metallplaadi sees, sobivad küll hästi madalama kristallumiskiirusega polümeerimaterjalide, näiteks polüpropüleeniga uurimiseks, kuid suure kristallumiskiirusega materjalide (nagu polüetüleen, polüamiidid, polüpiimhape jne) jaoks on tarvis teistlaadi insenerlikke lahendusi. Kirjanduses leidub üksikuid huvitavaid näiteid unikaalseadmetest, kuid igal neist on teatavad piirangud. Seega oli käesoleva töö ülesandeks välja töötada rutiinseks mõõtmiseks sobiv lahendus, mis võimaldaks polümeerse proovi temperatuuri muuta kiiresti, täpselt ja kontrollitult ning seejuures võimaldaks tema morfoloogiliste muutuste uurimist optiliste meetoditega, mis eeldab kuumutus- ja jahutuselementide läbipaistvust.

Kahe erineva meetodiga – kiipnanokalorimeetria ja kuumaluse polarisatsioonmikroskoopiaga tehtud uuring võrdlemaks polümeeride kristallisatsioonikäitumist mõõdukatel ja suurtel allajahutustel tõi ilmsiks kvalitatiivse erinevuse – suurtel allajahutustel kristallus unimodaalne materjal kiiremini kui bimodaalne, mis viitab kristallumismehhanismi muutusele allajahutuse suurenemisel. Uni- ja bimodaalse materjali kristallumiskiiruse temperatuurisõltuvuse interpolatsioonijooned lõikuvad ligikaudu 100°C kohal. See uuring osutab ühtlasi nende kahe isotermlise meetodi rakenduspiiridele temperatuuri skaalal.

Uut tüüpi seadme kontseptsiooni loomisel tuginedes kirjanduses viidatud ja varem samas laboris konstrueeritud kuumaluste parameetrite võrdlusele ja arvestati erinevate kütteviiside ja jahutuseks kasutatavate soojuskandjate efektiivsuse, temperatuurianurite tüüpide jne. mõju jahutuskiirusele ja täpsusele. Lähtuti eeldusest, et soojusliku inertsi vähendamiseks ja hea termilise kontakti huvides

peab objekti tugi olema ühtlasi küttekeha, seejuures võimalikult väikese massiga ja läbipaistev – näiteks metallikile, mis on sadestatud õhukesele klaasile, ja jahutusvedelik peab voolama selle klaasi all. Oodatava jahutuskiiruse saavutamiseks sobiva (maksimaalse) klaasipaksuse leidmiseks kasutati teoreetilist mudelit. Kütteelemendina katsetati vaakumaurustusel saadud poolläbipaistvat pidevat kullakilet, aga ka plasmapihustuse teel tekitatud vasekihist fotosöövitatud peenikest küttespiraali, samuti indium-titaanoksiidi (ITO) kilet. Temperatuuri mõõtmiseks katsetati peenikesest traadist lamedaks valtsitud termopaari polümeeriprooviga termiliselt ekvivalentses asukohas ja läbipaistava küttekeha enda takistuse temperatuurisõltuvust. Takistuse kaudu temperatuuri mõõtmine osutus oodatult kiiremaks ja töökindlamaks, küttekile materjalidest on ITO-l eelised nii läbipaistvuse kui morfoloogilise ja mehaanilise püsivuse osas. Klaasi paksuse mõju ületavaks osutus jahutuseks kasutatava soojuskandja mõju – vedeliku suurima efektiivsuse tingivad tema eelis massiülekanedega soojus eemale kanda ja samas suurem soojusmahtuvus kui gaasil. Katsest kasutada jahutamisel ka vedeliku aurustumissoojust loobuti tuleohtlikkuse ja sellest tingitud tehnilise keerukuse tõttu. Täpsuse ja kiiruse huvides kasutati spetsiaalselt konstrueeritud elektroonilist temperatuuri mõõtmise ja kontrolli süsteemi (kiirusega 3300 K/s ja maksimaalse tundlikkusega 10 V/1% takistuse muutuse kohta) ning National Instruments LabVIEW™ keskkonnas loodud virtuaalset instrumenti koos 16-bitise mõõtekaardiga firmalt Data Translation.

Töö tulemusena saavutati õhukesele klaasile sadestatud elektriliselt köetava ITO-kilega ja selle all voolava toatemperatuurse vedelikjahutusega seadmega reaalne jahutuskiiirus 500 K/s, mis ületab seniste kuumaluste maksimaalset jahutuskiirust 30 korda. Jahutuskiirust on võimalik kahekordistada eksponentsiaalselt sihtvõimsuseni kasvava kütterežiimiga ja vajadusel jahutusvedeliku temperatuuri alandamisega. Uudse tööpõhimõttega seade ja lihtne meetoodika võimaldavad suure kristallumiskiirusega polümeeride (näiteks polüetüleen) kristallisatsioonikäitumist optiliselt jälgida ja uurida senisest üle 25 K suurematel allajahutustel.

## **ABSTRACT**

### **Methodology and equipment for optical studies of fast crystallizing polymers**

The metastable morphology arising at the low temperatures of industrial crystallization process has a strong impact on the properties of a polymer product. High inherent crystallization rates make studies of some simple and wide-used polymers complicated at lower temperatures, where the rate increases considerably. Comparative crystallization study of two PE materials of different modality made by CNC and HS PLM revealed a qualitative difference between PE crystallization behaviour at higher and moderate supercooling and also demonstrated the limits of applicability of these two techniques in terms of temperature of isothermal analysis. The new solution for microscopy hot-stage design, based on electrically heated ITO-film on thin glass substrate and room temperature water-flow cooling together with a judicious control unit, yields a real cooling rate 30 times exceeding that of earlier solutions and, thus, broadens the routine applicability of optical methods of polymer (PE) crystallization studies for at least 25 K towards larger supercooling.